

**BLOOD COAGULATION TIME MEASUREMENTS
USING
400 MHZ THICKNESS MODE RESONATOR**



A Thesis

by

Negar Majidi

Submitted to the
Graduate School of Sciences and Engineering
In Partial Fulfillment of the Requirements for
the Degree of

Master of Science

in the
Department of Electrical and Electronics Engineering

Özyeğin University
August 2018

Copyright © 2018 by Negar Majidi

**BLOOD COAGULATION TIME MEASUREMENTS
USING
400 MHZ THICKNESS MODE RESONATOR**

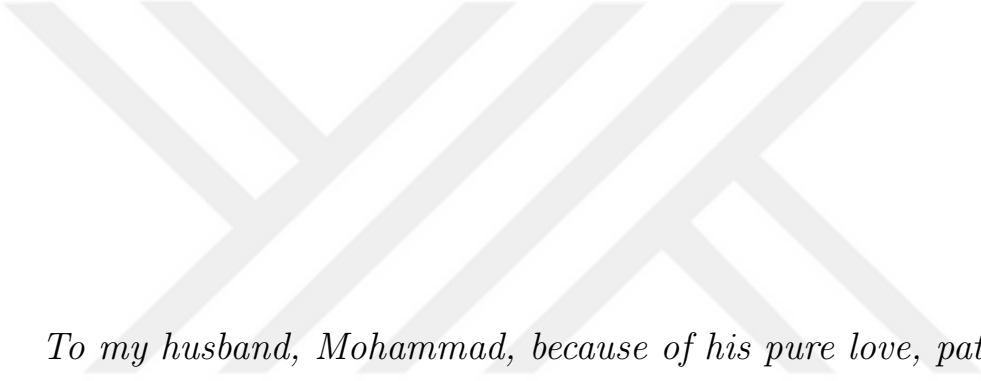
Approved by:

Professor G. Göksenin Yaralıođlu, Advisor
Department of Electrical and Electronics
Engineering
Özyeđin University

Professor H. Fatih Uđurdađ
Department of Electrical and Electronics
Engineering
Özyeđin University

Professor Ayhan Bozkurt
Department of Electrical and Electronics
Engineering
Sabancı University

Date Approved: 21 June 2018



*To my husband, Mohammad, because of his pure love, patience, and
endless encouragement...*

ABSTRACT

This thesis presents a novel blood coagulation time measurement methodology which requires as low as $1 \mu\text{L}$ of whole blood. The method performs measurements using whole blood without plasma separation. In this regard, the whole blood sample is placed on the top surface of a fused quartz plate (glass substrate) where an ultrasonic transducer (operating in thickness mode) is fabricated on the bottom surface. The transducer utilizes a short burst of 400 MHz compressional acoustic waves along the thickness of glass substrate. The location of the blood sample is aligned with the transducer; therefore, the reflected acoustic waves from the blood/quartz interface are captured and converted to electrical signals by the transducer. A Mason modeling of the transducer in frequency domain was expressed to show the changes of resonance frequency of the transducer for different samples, like air, water, and blood, alongside with a numerical modeling to show amplitude of acoustic waves propagating inside the transducer in time domain.

The acoustic impedance of the blood changes due to the coagulation process. This affects the reflection coefficient and amplitude of the reflected waves from the blood/quartz interface. A theoretical model was developed to show dependency of the acoustic waves amplitude to the reflection coefficient. Thus, the blood coagulation time was determined by monitoring the reflected acoustic waves amplitude. The transducer was made of $8 \mu\text{m}$ thick of sputtered Zinc Oxide (ZnO) thin-film that is operating at approximately 400 MHz TE (Thickness Extensional) mode.

In the experiments, whole blood sample was used without any preparation. The method was tested using citrated blood with calcium chloride and activated partial thromboplastin (aPTT) reagents. We observed that aPTT coagulation times lengthen

from 25 sec. to 47 sec. with the addition of heparin. The proposed method has a potential to be used in a disposable low cost portable coagulation time measurement cartridge for patient self-testing. The measurements were performed by collecting the amplitude of the reflected waves versus the time at specific frequency (400 MHz); however, another possible way could be using a simple oscillator and a digital counter to track the resonance frequency and quality factor of the transducer versus the time. This will further reduce the cost and size of the proposed method. Nevertheless, this transducer has a potential to be used for characterizing liquid samples parameters like viscosity, if it is operated in frequency domain and the input impedance is being tracked. This could be used for the applications where the lower volume of an expensive drug or chemical to be tested, is mostly desired.

ÖZETÇE

Bu tez, yeni bir kan pıhtılaşma süresi ölçüm metodolojisi sunmaktadır. Metod plazma ayırımı olmaksızın 1 mikro L tam kan gerektirir. Bütün kan örneği, ultrasonik güç çevirici (kalınlık modunda çalışan) ile birleştirilmiş bir kuvars plakanın üst yüzeyine yerleştirilir (cam alt tabaka). Dönüştürücü 400MHz'lik kısa bir sinus dalgaları üretir. Bu dalgalar cam alt tabakanın kalınlığı boyunca akustik dalga olarak yayılır. Kanın yeni örnek dönüştürücü ile hizalanmıştır; Kan/kuvars yüzeyinden yansıyan dalgalar yeniden dönüştürücüyü tarafından toplanır ve elektiksel sinyallere çevirilir.

Bu tezden dönüştürücü frekans alanında Mason modellemesi ile ifade edildi. Farklı örnekler için transdüserin rezonans frekansındaki değişimleri incelendi, hava, su ve kan gibi malzemelerden gelen yansımalar zaman alanında hesaplandı. Kanın akustik empedansı, pıhtılaşma sürecine bağlı olarak değişir. Bu Yansıyan dalgaların fazını ve genliğini değiştirir. Değişim hesaplanması için teorik bir model geliştirildi. Böylece kan pıhtılaşması akustik dalgaların izlenmesiyle ölçülebilir.

Transdüser, 8 mikro- metre kalınlığında püskürtülmüş Çinko Oksit'ten (ZnO) yapılmıştır. Yaklaşık 400 MHz TE (Kalınlık Uzama) modunda çalışır. Deneylerde, tam kan örneği herhangi bir örnek hazırlama basamağı olmaksızın kullanıldı. Yöntem kalsiyum klorür ile sitratlanmış kan ve tromboplastin (aPTT) reaktifleri kullanılarak test edildi. Heparin ilavesi ile aPTT pıhtılaşma sürelerinin 25 saniyeden 47 saniyeye uzadığını gözlemlendi. Önerilen yöntem Tek kullanımlık düşük maliyetli taşınabilir pıhtılaşma süresi ölçümünde kullanılabilir. Pıhtılaşma zamanı rezonans frekanı ve kalite izlemek gibi yöntemlerle de ölçülebilir. Pıhtılaşma zamanı yanında önerilen metod sıvıların karakterizasyonu için de kullanılabilir.

ACKNOWLEDGEMENTS

I would like to thank my supervisor Dr. Göksenin Yaralıođlu for his patience, support and guidance. I am grateful to my parents, MohammadAli and Ashraf for their love and supports. I would also like to thank my colleagues and friends at OzU, SeyedFakhreddin Nabavi, Erkan Kemal, and Hakan Çetin in general, and special thanks to administration staffs, Aylin Muhaddisođlu and Gizem Bakır in particular for their supports.

I also thank my thesis jury for their guidance and interests in my research filed.

Last, but not the least, I express my gratitude to my husband, Mohammad, for his aid and understanding throughout of my graduate education and research.

TABLE OF CONTENTS

DEDICATION	iii
ABSTRACT	iv
ÖZETÇE	vi
ACKNOWLEDGEMENTS	vii
LIST OF TABLES	x
LIST OF FIGURES	xi
I INTRODUCTION	1
1.1 Blood Coagulation	1
1.2 Ultrasound and Principles of Proposed Method	3
II PIEZOELECTRICITY	6
2.1 Piezoelectric Materials	7
2.2 Thin-Film Thickness-Mode Sensors	8
2.3 Mason Modeling	10
III BLOOD COAGULATION MEASUREMENT METHODS BY ULTRASOUND	15
3.1 Acoustic Waves Speed	15
3.2 Ultrasound Attenuation	17
3.3 Ultrasound Backscatter	19
IV ZNO BASED SM BAWR AND BLOOD COAGULATION TIME MEASUREMENT	21
4.1 Materials and Methods	23
4.1.1 Thickness Mode Solidly Mounted Resonator (Ultrasounic Transducer)	23
4.1.2 Circuitry	23
4.1.3 The Temperature Control System	25
4.1.4 Pulse-Echo Measurements	26

4.1.5	Blood Sample Preparation	30
4.1.6	Numerical Modeling of th Acoustic Waves Propagation . . .	31
4.1.7	Mason Modeling and Resonance Frequency	35
4.1.8	Results and Discussions	42
V	CONCLUSION	47
	REFERENCES	49
	VITA	52



LIST OF TABLES

- | | | |
|---|--|----|
| 1 | Mechanical and acoustical properties of water, whole blood, and air. . . | 38 |
| 2 | Some properties of used materials in simulation and calculations. . . . | 39 |



LIST OF FIGURES

1	Structure of BAW resonator.	8
2	Magnitude of input impedance of BAW resonator.	9
3	Illustration of some different 1-D mode of resonating.	10
4	Piezoelectric crystal orientation and resonating mode.	11
5	Two common topologies for TE mode resonators; FBAR (Thin-Film Bulk Acoustic Resonator) on left; Solidly Mounted Resonator with multiple back reflectors on right.	11
6	Cross section of Thickness Excitation mode PE transducer.	12
7	Mason's equivalent circuit for TE mode oscillating PE transducer. . .	14
8	Four channel sound speed measurement chamber for whole blood coagulation [46].	16
9	(a) speed of sound obtained by four different channels; (b) integral of the curve for one channel [46].	17
10	Diagram of transducer based on attenuation [47].	18
11	RMS value of reflected acoustic waves traveling into the blood sample [47].	19
12	A typical ultrasonic image during the blood coagulation [48].	20
13	(A) Side view of the cartridge; (B) Top view of the cartridge. The electrical connections were not shown.	24
14	Bottom view of the fabricated ultrasonic transducers on the fused quartz substrate. The ground electrode is the same for all the transducers and it runs in the horizontal direction over the zinc oxide film. Other electrodes are between the zinc oxide film and the substrate. . .	25
15	(A) Block diagram of the electronics set-up for pulse echo measurements; (B) A photo of the measurement set-up.	26
16	The commercial temperature control system for keeping the temperature at $37 \pm 0.5^\circ\text{C}$	27
17	Simplified drawing of acoustic reflections in the cartridge, where R1 is the first reflection from boundary of the quartz substrate and the blood sample.	28

18	(A) Multiple reflections in the quartz substrate for Air and DI water; (B) The zoomed R1 pulses for Air, DI water, and Ci-Blood. The acoustic waves reflect in the quartz substrate multiple times and decay due to the acoustical and diffraction losses. Time delay between each reflection is around 440 ns which is proportional to the longitudinal sound speed (5500 m/sec) and thickness of the fused quartz (1.2 mm).	29
19	The computed RMS value of reflected R1 pulse, while a drop of DI water was put on the quartz substrate.	30
20	The simplified modeling of the proposed disposable cartridge and liquid sample. The compressional vibration of the transducer is modeled as two mechanical pressure in opposite direction.	32
21	Comparison of the practical measurement versus the numerical modeling, when there is no liquid on the quartz (medium is air). The amplitude for the both practical and modeling results are almost same along the three reflections.	36
22	The transducer and mediums as acoustical layers.	37
23	Absolute value of input impedance versus frequency.	40
24	Phase of input impedance versus frequency.	41
25	Maximum TE displacement of the transducer at resonance frequency, simulated in COMSOL.	42
26	Absolute value and phase of Input impedance of the transducer for multiple resonance frequencies without considering the loss effect. . .	43
27	Comparison of resonance frequency and quality factor for three different droplet samples.	44
28	The calculated RMS value of raw and fitted curves of R1 for aPTT tests. Only one set was shown in this figure. We repeated each test 5 times. As heparin volume increases in the blood mixtures, settling time (or coagulation time) also increases.	45
29	The computed coagulation time measurement based on the average, minimum, and maximum values for three different concentrations of blood and heparin mixtures.	46
30	Asymmetric oscillator circuit.	48

CHAPTER I

INTRODUCTION

The POC (point-of-care) applications of MEMS (Micro Electro Mechanical System) devices are drawing more attention in the last decades, while the fabrication methods and trends enable micro/nano facilities to build and fabricate cost effective, much smaller and more accurate devices. These everyday expanding technologies enable biomedical researchers to fabricate cheap and disposable Point-of-Care devices to ease the diagnostic processes for patients and medical centers. A portable blood sugar measuring device with disposable cartridge or blood coagulation measurement biosensors are examples of mostly demanded POC applications which people are using widely in their life. However, these POC kits still need to be further miniaturized.

Usually the main part of these devices is a sensor which converts a biological activity to a mechanical or electrical measurand and vice versa. The quality of these transducers depends on the size, used materials, device structure and topology, and other basic physics and chemistry principles. Nowadays, the most biosensors have been fabricated based on photonics and opto-electronics, mechanical vibrations, RF proximity, and ultrasound transducers.

1.1 Blood Coagulation

Blood clotting, which occurs to stop bleeding, is a result of a consecutive biological interactions. Coagulation time is a vital indicator of specific factors in blood and their adequacies. In this regard, various tests are performed at hospitals, where requires patients to travel to these medical centers. Although, portable healthcare kits have been developed to identify amount of these factors, but the amount of the blood required for existing devices (5 to10 uL) usually cannot be provided by a simple

finger prick which is crucial for some groups of patients, like a dialectician.

The major portable blood coagulation time detection methods can be classified into four major groups:

1) Optical sensing: in this approach, optical intensity is measured. Optical properties (usually fluorescence) of the added reagents into the blood plasma change due to the chemical changes that occur during coagulation. A spectrophotometer measures coagulation time by detecting optical intensity variations at different wavelengths. This approach is widely used in hospital or lab-based instruments [5,6] but it requires a centrifuging step to separate plasma from blood.

2) Electrical sensing: these methods are based on detecting impedance change of blood. Since they do not require large optical components and sample preparation, these methods are used in portable devices [7,8]. However, both optical and impedance measurement approaches are indirect since they measure a secondary effect that is introduced by the blood coagulation. Direct methods on the other hand measure the viscosity change of the mechanical properties of blood during coagulation. So, they are more dependable and immune to other factors such as high fat concentration that may affect optical and electrical properties of blood.

3) Mechanical sensing: mechanical sensing methods can be considered as a direct approach and they measure dynamics of a moving structure in blood sample. For instance, motion of a cantilever is monitored in a blood sample while clotting process is occurring [9,10].

4) Ultrasound sensing: these methods use ultrasonic waves to measure amplitude and phase change of ultrasonic waves propagating in a blood sample. Reflected acoustic waves from a sample can provide invaluable information such as sound velocity, temperature and viscosity of blood [11,12]. However, these methods usually require a large volume of blood and have low chance to become a portable device.

In this dissertation, we present a $500\ \mu\text{m}$ by $500\ \mu\text{m}$ transducer fabricated on a

glass substrate which operates at 400 MHz thickness mode. The proposed transducer was used to measure the blood coagulation time measurements by measuring the amplitude of the reflected acoustic waves coming from glass and 1 μL of whole blood droplet boundary interface. Although the amplitude of the acoustic waves are captured versus the time, however, the proposed transducer can be connected to a simple oscillator and a digital counter to track resonance frequency of the transducer versus the time. This will further reduce the cost and size of the proposed method.

1.2 Ultrasound and Principles of Proposed Method

Ultrasound is an acoustic wave with an oscillating frequency of 20 KHz and greater. The ultrasound was first used for the medical and diagnostic purposes in 1940 by collecting the reflected waves versus the time (A-Scan mode) [1]. The acoustic waves are the results of vibration of adjacent molecules of a medium. Based on direction of the wave vibration and propagation, few different acoustic waves can be considered. However, the most used acoustic mode in biomedical imaging and industrial applications is Longitudinal (or Compressional) wave where the acoustic waves propagate in the same direction of the molecular vibration. The ultrasound waves can be generated in few common waves:

- 1) Using specific speakers which mechanical movements of diaphragm applies continuous back and forth forces to a medium mostly for airborne applications.

- 2) Piezoelectric material which changing the voltage over two side of it, changes the ceramic shape and reversely, squeezing the ceramic produces voltage on it.

- 3) CMUT technology where the applied voltage over the plates of a capacitor generates an electrostatic force and cause the movement of plates. Usually a single ultrasound transducer can be used in both transmit and receive mode as an ultrasound transceiver.

Since the wave length of a propagating acoustic waves are usually much smaller

than the medium length, so the impedance and reflection coefficient of the interfaces need to be considered and have crucial effect on the quality of acoustic waves. For a compressional wave, in an operation frequency range of few Mega Hertz, the acoustic impedance of a medium becomes the product of density by acoustic wave speed. Although the viscosity and attenuation of the medium have effect on the acoustic impedance, for a low frequency of few MHz, these effects can be neglected. The amplitude of reflected acoustic waves is directly related to the acoustic impedance mismatch of two layers; the greater impedance mismatch, the greater amplitude of reflected waves. In this thesis, the amplitude of the acoustic waves reflected by an interface of glass substrate and blood sample was recorded versus the time to track the blood coagulation time.

The quality factor, operation frequency, ease of fabrication, and cheap fabrication methods of the transducer to be used in this work are very important. The Solidly Mounted Bulk Acoustic Wave Resonator is an excellent choice for these highly demanded upcoming technologies such as RF filters and gravimetric biosensors, due to their ease of fabrication, CMOS compatibility, high quality factor, and power handling. Regardless of resonating modes, to yield a high-quality factor BAW device, the acoustic energy must be trapped inside the bulk piezoelectric film by using either multiple mismatch reflective layers or air gap. However, this enormous dependency of the BAW performance to the acoustic impedance of the adjacent layers (or mediums) may be adequate to consider these devices as a sensor for mediums impedance investigations. Nevertheless, the BAW devices operating in TE modes are more sensitive to immersed environments where sharing a common acoustic interface with liquid medium. Therefore, the TE mode BAW devices have a potential to be used for liquid impedance determination by investigating the resonator parameters such as input impedance and quality factors.

In the following sections the basic of Piezoelectricity, Bulk Acoustic Wave Resonators (BAWR), set-up and results of practical measurements, and analytical simulations of the proposed method will be presented. f



CHAPTER II

PIEZOELECTRICITY

By the early 1980s, devices fabricated based on acoustic transducer had shown themselves to be quite suitable for many technical applications, especially in electronics, data processing and high frequency technologies. The increasing demands of commercial products in the telecommunication area provided the basis to use mass-produced surface acoustic wave (SAW) devices for the frequency range of 100 MHz to a few GHz. In practice, the SAW devices generate and detect acoustic waves using interdigital transducers (IDT) on the surface of a piezoelectric material [22]. In this way, the acoustic energy is strongly confined at the surface of the device (piezoelectric) in the range of couple acoustic wavelength, regardless of the thickness of the complete piezoelectric [23]. Because of that, the propagating waves on the surface are potentially very sensitive towards any change on the surface, such as pressure, mass loading, viscosity of the liquid in touch with the surface. Wohltjen and Dessy first presented a sensor based on a SAW which was coated with a sensitive polymer layer. It was used as a chemical sensor for organic gas detection [24, 25].

However, early attempts to apply this innovative technology into a biosensor to detect proteins were not quite successful [26-28]. The reason for the failure is that to achieve this application, the device usually must be operated in touch with solutions. When the device is immersed in aqueous liquids, the SAW devices commonly used for gas sensing suffer from attenuation due to displacement components perpendicular to the surface. The SAW devices were first used as telecommunication filters. But because of the highly temperature sensitivity and lower Q , the SMR-BAW devices are an excellent choice for upcoming technologies due to high Q and power

handling. Thus, research activity was largely focused on bulk acoustic waves (BAW). The devices commonly known as quartz crystal microbalances (QCM) [29-33]. The resonance frequencies of these devices are usually in the range of 10 to 50 MHz.

The main differences between SMR (Solidly Mounted Resonator) or BAW (Bulk Acoustic Wave) devices and FBARs (Thin-Film Bulk Acoustic Resonators), is the way that acoustic energy is trapped in bulk. In SMR, lower level reflectors trap this fundamental mode. These reflectors must be designed very well, otherwise will cause a degradation in both coupling coefficient and Q. Similarly, in FBARS, the Air and crystal interface on both faces trap the main mode of resonator. At higher frequencies the BAW and FBAR devices must to be too thin and thus too fragile for practical use. However, the mass sensitivity of the devices increases by operating frequency [34]. This said, compared to SAW devices, both FBAR and BAW devices offer higher power handling, temperature stability, and higher Q especially in immersed environment.

2.1 Piezoelectric Materials

The word of Piezoelectricity means generating the electricity by applying pressure. The name and principles of the piezoelectricity was first discovered in 1881 [19, 20]. The term of piezoelectricity is used to describe dielectric materials that produce electrical charges across their boundaries due to the applied mechanical stress, which is called the direct piezoelectric effect [21]. In simple words, if a piezoelectric material is bended, pushed, or pulled, an electrical voltage will be generated and conversely by applying a voltage to a piezoelectric material, the material will be reshaped. For the case of longitudinal mode resonators made of piezoelectric materials, the following equations can be written:

$$\begin{aligned} S_3 &= s_{33}^E \cdot T_3 + d_{33} \cdot E_3 \\ D_3 &= d_{33} \cdot T_3 + \epsilon_{33}^T \cdot E_3 \end{aligned}$$

where the notation of 3 means z-axis; where S is strain, s_{33}^E is compliance, T is stress,

d is charge-form piezoelectric constant, E is the electric field applied to resonator, D is electric density displacement, ϵ_{33}^T is permittivity of the piezoelectric material.

2.2 *Thin-Film Thickness-Mode Sensors*

A bulk acoustic wave resonator consists of a thin film of piezoelectric material which is sandwiched from both sides for applying an electrically exciting voltage as illustrated in Figure 1. The thin film resonates whenever an integer multiple of half an acoustic wavelengths fits within the resonator thickness t :

$$f_N = vN / 2t$$

where v is the shear or longitudinal acoustic velocity, N is an integer multiplier, and t the thickness of the thin film. Only odd values of N generates a resonating but even N corresponds to antisymmetric modes. The electrical modeling of a resonator, resonating near to the fundamental frequency is shown in Figure 2 where f_r and f_a represent the resonance and anti-resonance frequencies. Resonators with very low losses yield a high Q -value resonator.

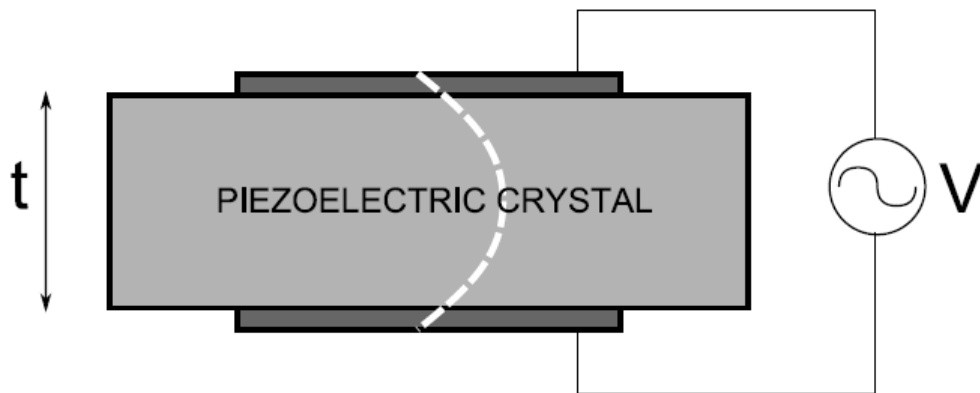


Figure 1: Structure of BAW resonator.

The traditional method of fabricating crystal oscillators from a bulk crystal is dicing a thin layer of crystal and then polishing to attach the electrodes. In this

method, it is difficult to dice very thin layer of a crystal which limits the operation frequency below 200MHz.

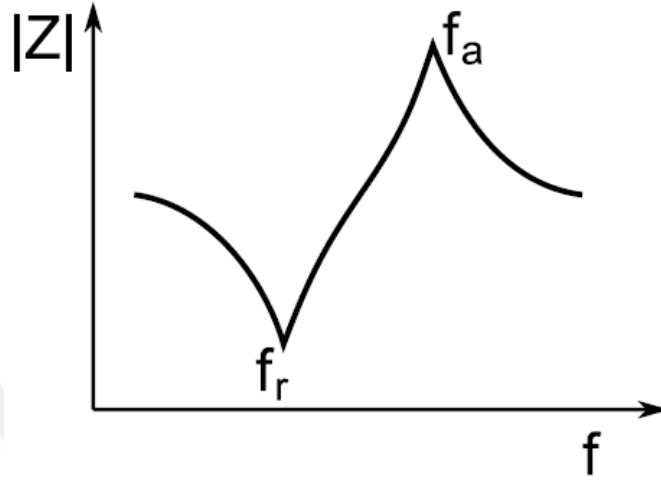


Figure 2: Magnitude of input impedance of BAW resonator.

The thin-film bulk acoustic wave resonator is based on the same principal structure, but the piezoelectric material are produced by deposition of thin film in vacuum chamber. This further reduces the thickness of piezoelectric films to operate in range of up to 15 GHz. Standard lithography and etching methods can be used for fabrication of these devices. However, the deposition parameters and quality of the seed layers are playing critical role to determine the resonating mode of the transducer by changing the angle of crystal.

Figure 3 shows few 1-dimensional resonating mode and Figure 4 demonstrates the relation between angle of crystal and resonating mode. The piezoelectric thin films such as ZnO and AlN exhibit a much stronger piezoelectric effect than traditional quartz and require highly oriented c-axis (002 plane) to operate in Thickness Extensional Mode, as we did in this thesis. Figure 5 illustrates two different common topologies of the BAW resonator; SMR (Solidly Mounted Resonator) and FBAR

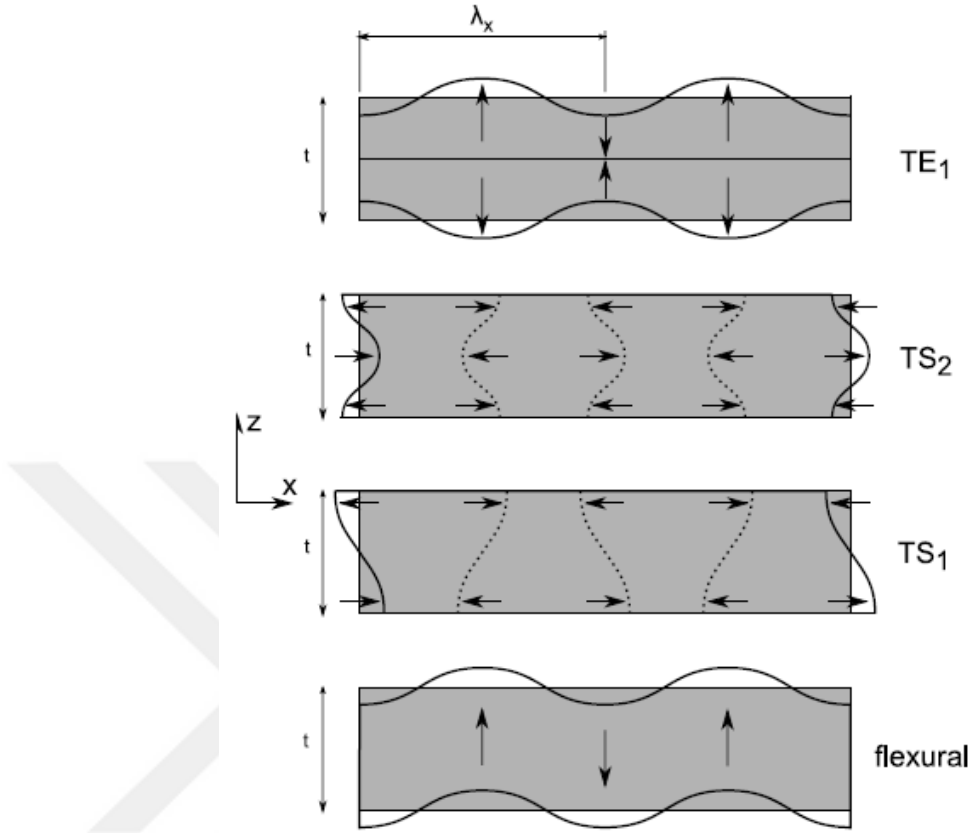


Figure 3: Illustration of some different 1-D mode of resonating.

(Thin-Film Bulk Acoustic Resonator). Basically, the FBARs have higher quality factor rather than the SMR, because of lower acoustical loss in layers. However, the fabrication of SMR devices are much easier.

2.3 Mason Modeling

Piezoelectric materials convert mechanical energy into electrical energy and vice versa. The direct piezoelectric effect is based on the change in polarization in a material induced by an applied stress, and is used in the ultrasonic (transducer) reception stage. The converse piezoelectric effect is based on the mechanical strain in a material induced by an applied electric field, and is used in the ultrasonic (transducer) emission stage. The linear piezoelectric equations define the relationships among the electric

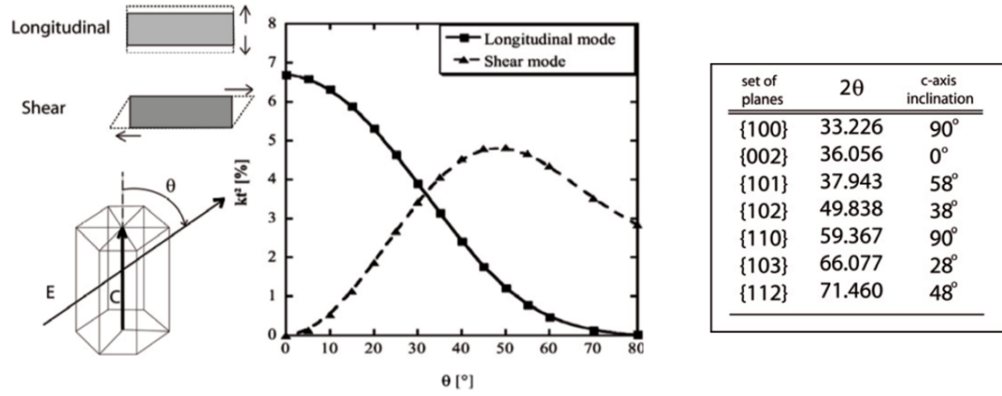


Figure 4: Piezoelectric crystal orientation and resonating mode.

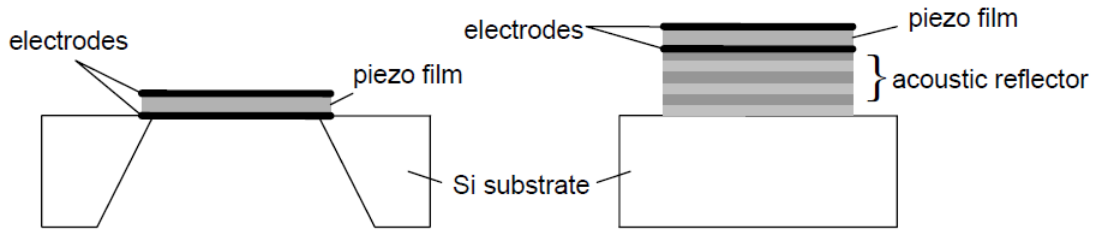


Figure 5: Two common topologies for TE mode resonators; FBAR (Thin-Film Bulk Acoustic Resonator) on left; Solidly Mounted Resonator with multiple back reflectors on right.

displacement D , the electric field E , the elastic strain S , and the mechanical stress T , as shown below. The parameters involved in the equations depend on the symmetry of the PE material and the geometry of the transducer element [35-39].

$$T_3 = c_{33}^D S_3 - h_{33} D_3$$

$$E_3 = -h_{33} S_3 + \frac{D_3}{\epsilon_{33}^S}$$

Figure 6 shows a diagram of the cross section of a thin film piezoelectric transducer. The electrical field is applied along the Z direction as same as the stress direction (thickness excitation mode). The notations 3 mean the applied electrical field and

mechanical stress both are in z axis (TE mode). This transducer can be considered as a three port device, with one electrical port, and two mechanical ports. These mechanical ports corresponding to the back (FB, u_B) and front (FL, u_L) forces F and particle velocities u at two faces.

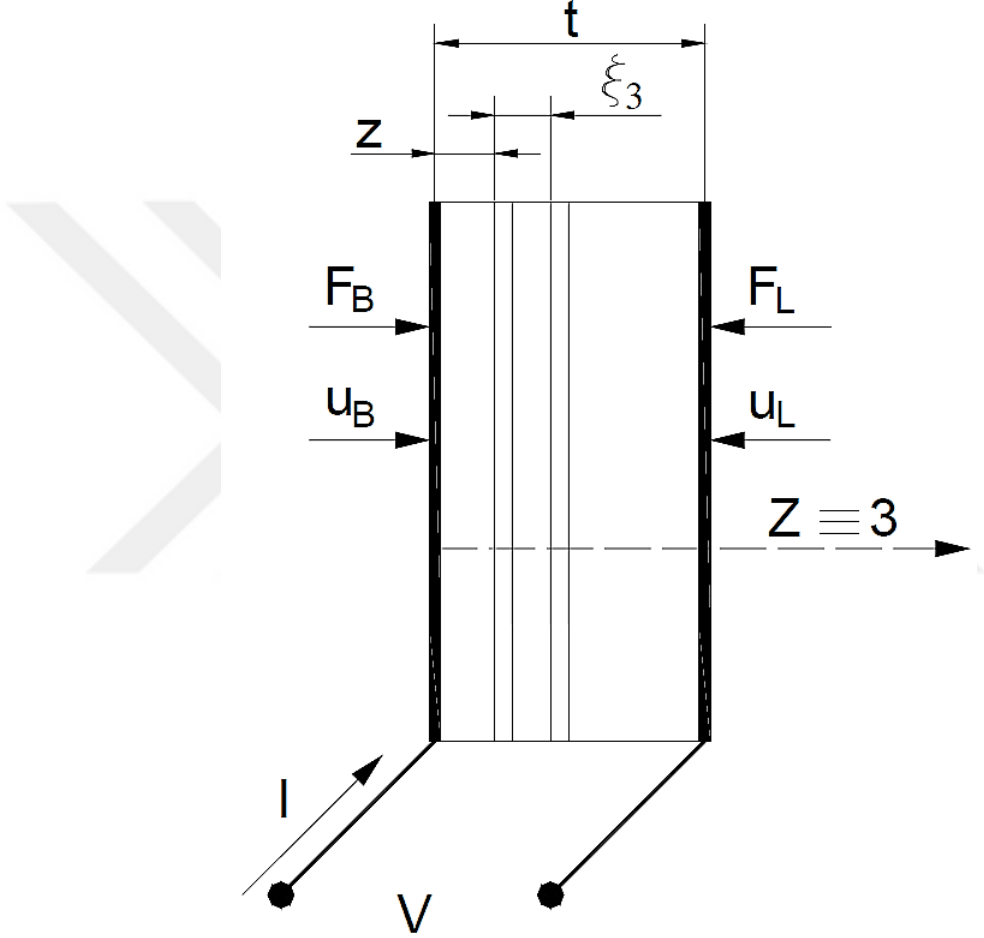


Figure 6: Cross section of Thickness Excitation mode PE transducer.

The corresponding equations for the transducer can be written in matrix form below where where c_{33}^D is the elastic stiffened constant ($c_{33}^D = c_{33} + e_{33}^2/\epsilon_{33}^S$), $h_{33} = e_{33}/\epsilon_{33}^S$ is the piezoelectric constant (e_{33} is the piezoelectric stress constant), ϵ_{33}^S is the clamped dielectric constant, $C_0^S = A\epsilon_{33}^S/t$ is the clamped (zero strain, high frequency) capacitance of the piezoelectric plate, A the area of the electrodes, $Z_0 =$

$(\rho c_{33}^D)^{1/2}$ is the characteristic stiffened acoustic impedance of the piezoelectric material. The characteristic impedances of the load is $Z_L = (\rho c_L)^{1/2} = F_L/(Au_L)$ and the backing is $Z_B = (\rho c_B)^{1/2} = F_L/(Au_L)$, being c_B and c_L the corresponding elastic constants [39].

$$\begin{pmatrix} F_L \\ F_B \\ V \end{pmatrix} = \begin{pmatrix} Z_0 A / j \tan \beta t & Z_0 A / j \sin \beta t & h_{33} / j \omega \\ Z_0 A / j \sin \beta t & Z_0 A / j \tan \beta t & h_{33} / j \omega \\ h_{33} / j \omega & h_{33} / j \omega & 1 / j \omega C_0^S \end{pmatrix} \begin{pmatrix} u_L \\ u_B \\ I \end{pmatrix}$$

Mason equivalent circuit modeling can be obtained by using the electromechanical analogy as shown in Figure 7 which has been widely used for PE transducer modeling, simulation, design, and optimization [40-42]. This equivalent circuit can be connected to any kind of loading in both sides where the Input impedance can be derived following where $k_t = h_{33}(\epsilon_{33}^S/c_{33}^D)^{1/2}$ is the electromechanical coupling coefficient.

$$Z_{in}(\omega) = \frac{1}{j \omega C_0^S} \left(1 + \frac{k_t^2}{\beta t} \frac{j(Z_L + Z_B)Z_0 \sin \beta t - 2Z_0^2 (1 - \cos \beta t)}{(Z_0^2 + Z_L Z_B) \sin \beta t - j(Z_L + Z_B)Z_0 \cos \beta t} \right)$$

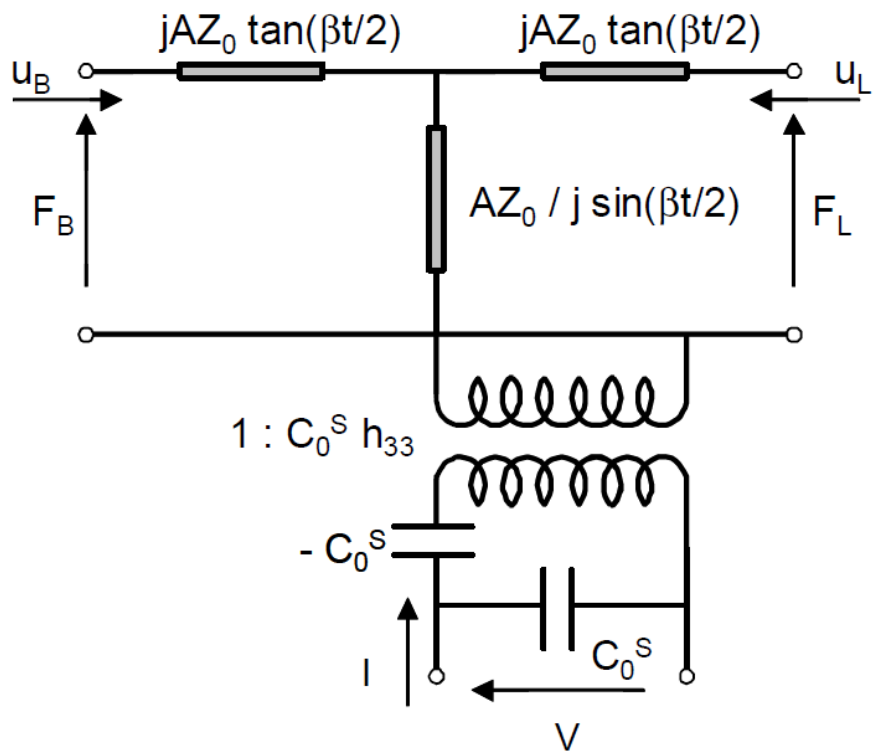


Figure 7: Mason's equivalent circuit for TE mode oscillating PE transducer.

CHAPTER III

BLOOD COAGULATION MEASUREMENT METHODS BY ULTRASOUND

Blood coagulation is a major defense mechanism that helps to stop blood loss from an injured vessel. Blood coagulation measurements performed in clinical laboratory usually observe the amount of vitamin K in the blood and health of liver. The coagulation of blood is a quite complex process which solid fibrins play important roles in this process, and can be affected by an imbalance coagulant and anticoagulant factors. A common method to measure the blood coagulation involves adding the blood to four test tubes and then tilting the tubes at 30-40 seconds intervals until the blood can no longer flow [43]. However these old methods require few mili liter of blood to be processed.

Blood coagulation measurement methods based on the ultrasound, usually require lower amount of the blood because of the smaller acoustic wave length inside the blood sample. These methods commonly utilize an acoustic wave into the coupled blood sample (or container) and on the receive side, track the changes on reflect acoustic properties, such as wave speed, attenuation, phase shifts, and etc. In this chapter just few ultrasound methods will be presented. However, many aspects of studying blood coagulation by ultrasound remain to be investigated since new discoveries often raise more questions than they answer.

3.1 Acoustic Waves Speed

Speed of an acoustic longitudinal wave vary with mechanical/acoustical properties of the medium (tissue or blood sample). Speed of sound is inversely proportional to the

compressibility of the tissue and density. Therefore, the sound speed propagating into the blood sample changes with blood coagulation processes. The velocity of the sound increases by blood coagulation [44, 45]. Figure 8 demonstrates an example of acoustic sound monitoring for blood coagulation purposes where 4 transducers were coupled to a tube and speed of sound for a round trip traveling was calculated versus the time [46]. The method was using 1 mL of blood with 4 active ultrasound transducers. The result obtained by this method is illustrated in Figure 9 for all the transducers. Speed of sound increases as the blood becomes more dense and solid (coagulating). The coagulation time is roughly 33 minutes.

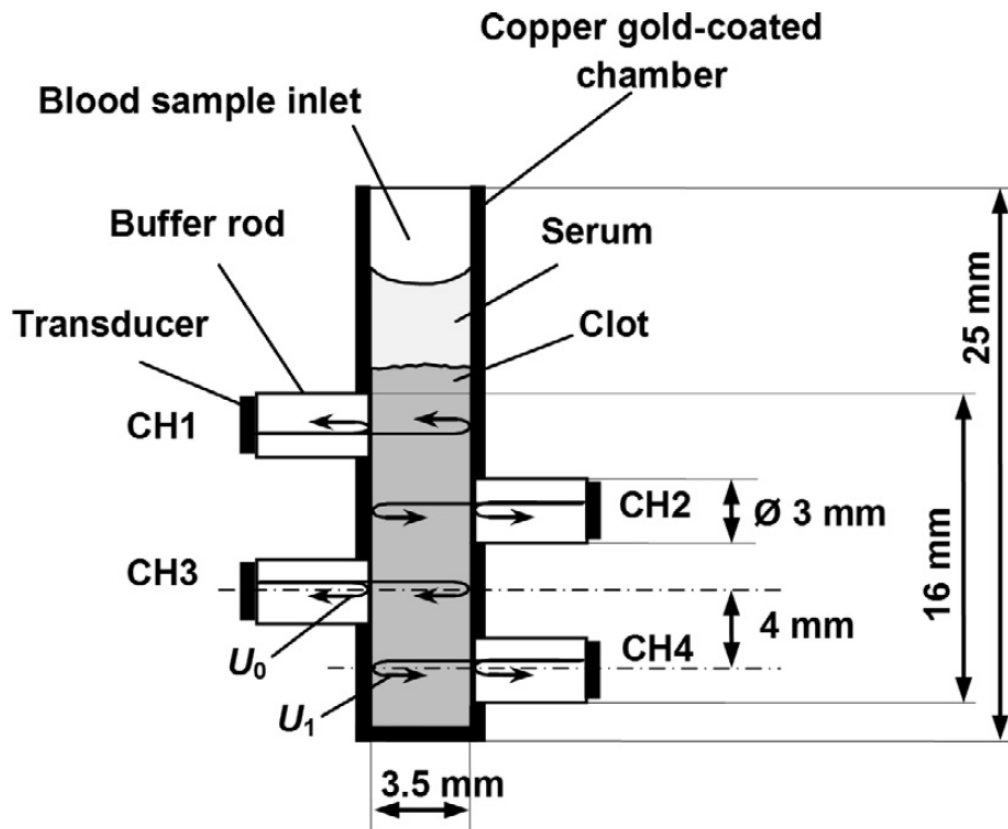


Figure 8: Four channel sound speed measurement chamber for whole blood coagulation [46].

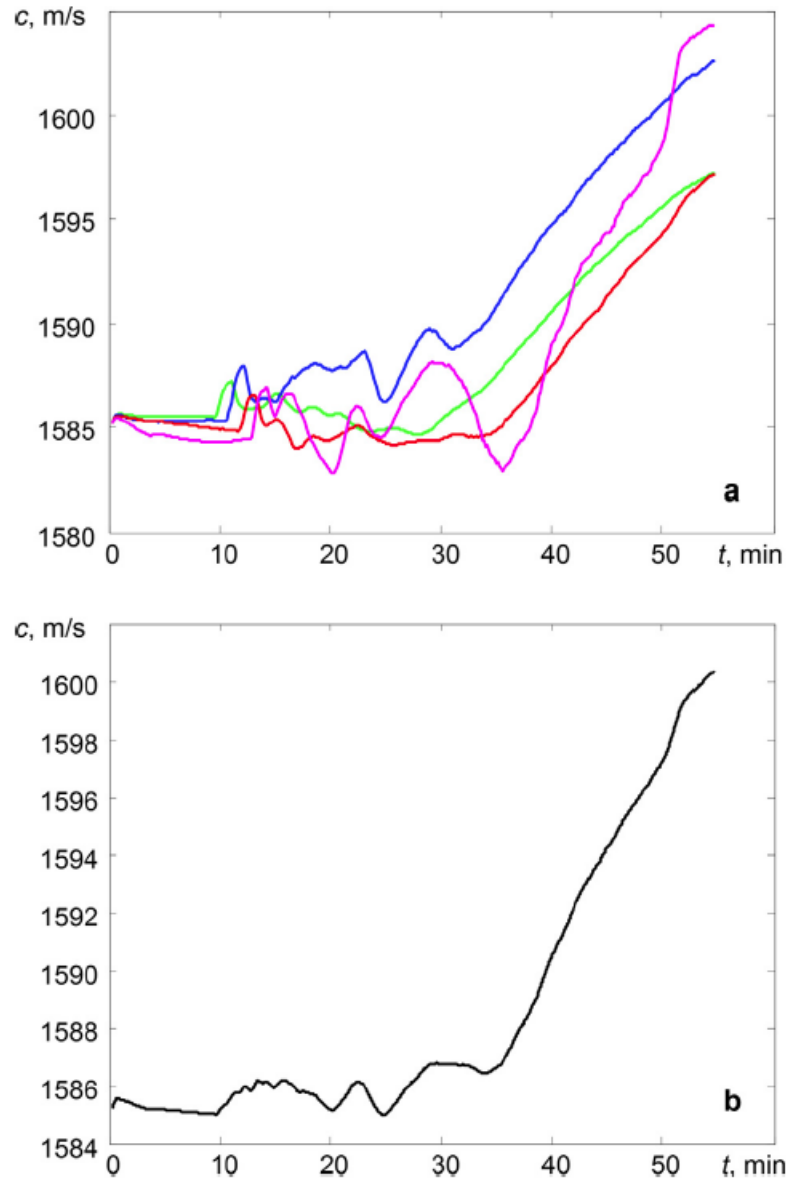


Figure 9: (a) speed of sound obtained by four different channels; (b) integral of the curve for one channel [46].

3.2 *Ultrasound Attenuation*

Some of the Ultrasound energy propagating in blood sample (tissue) is lost due to the reflection, scattering, and sample absorption. Attenuation increases by clotting the blood. This decreases the total energy of acoustic waves on the receive side.

Few measurements were done for attenuation of 10-30 MHz transducer by adding the heparin to human and rat blood [45]. Also another research was conducted to measure the amplitude of the reflected acoustic waves traveling into the blood sample by higher ultrasound transducer [47]. Although this research was not calculating the exact attenuation, but showing the amplitude that is inversely related to the attenuation. Figure 10 and 11 illustrates the diagram and obtained results for this research. However this method was very sensitive to the channel height and because of diffusion, blood rec cells can remain outside the channel.

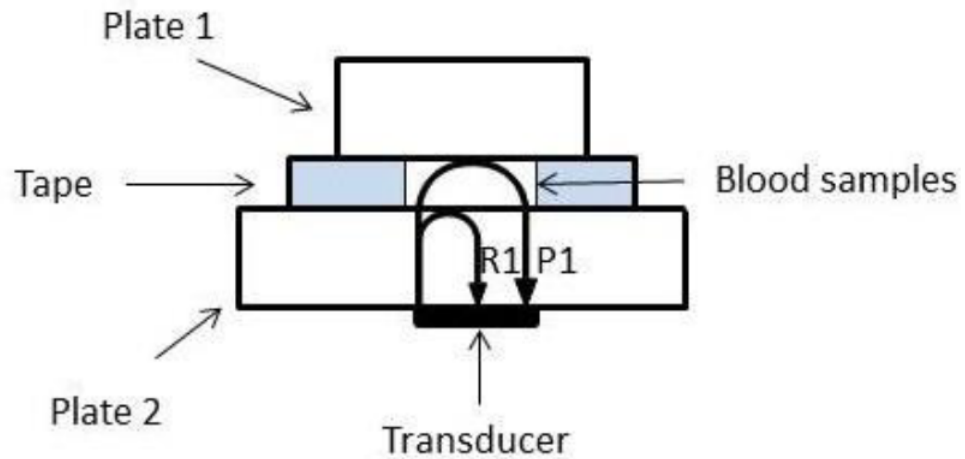


Figure 10: Diagram of transducer based on attenuation [47].

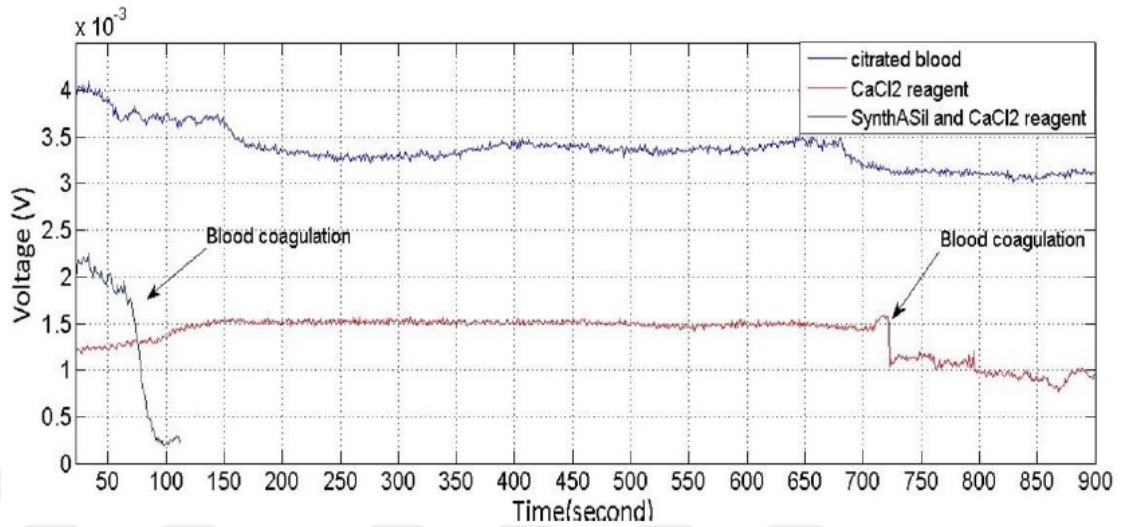


Figure 11: RMS value of reflected acoustic waves traveling into the blood sample [47].

3.3 *Ultrasound Backscatter*

When an ultrasound wave travels through a tissue (blood) its energy may be reflected or absorbed by the medium. Scattering will occur inside the medium if the particles are much smaller than the acoustic wavelength. These scattering of ultrasound can be captured by an imaging transducer to generate an image. This method has been used widely, but still it requires few milli liter of blood sample. Figure 12 shows an ultrasonic image obtained by backscattering versus the time. Coagulation occurs approximately at 2200 sec where the fibrins inside the blood remain stable and gel liquid is formed [48].

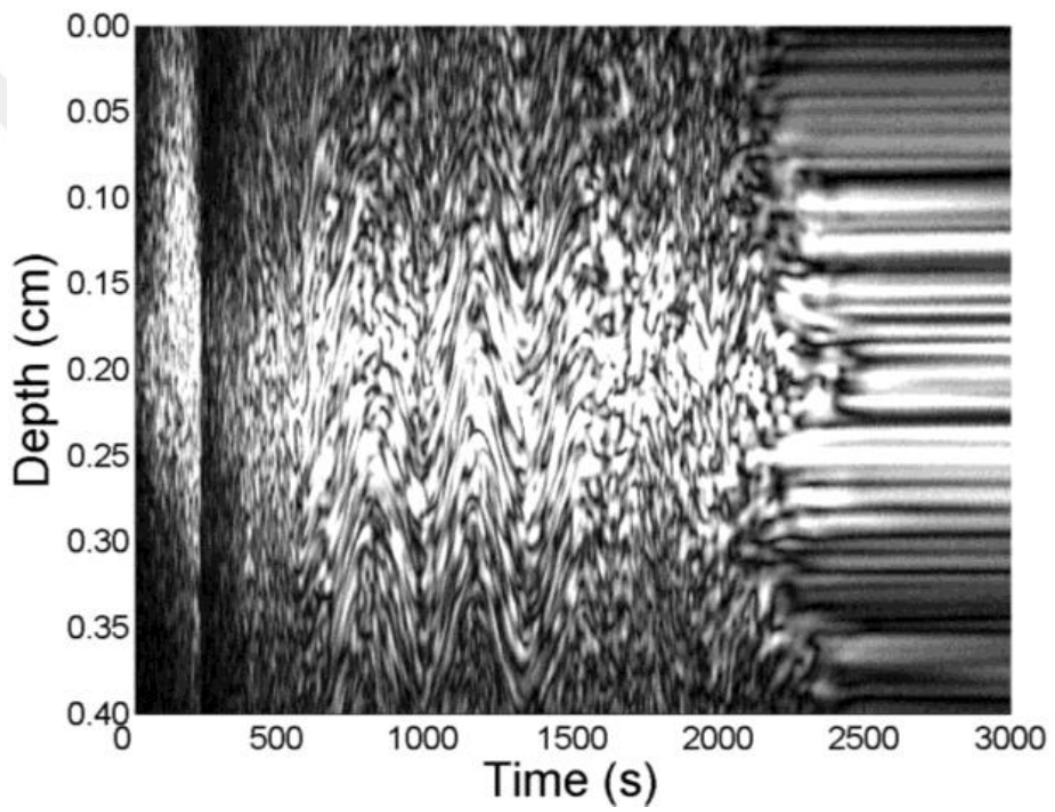


Figure 12: A typical ultrasonic image during the blood coagulation [48].

CHAPTER IV

ZNO BASED SM BAWR AND BLOOD COAGULATION TIME MEASUREMENT

Blood clotting, which occurs to stop bleeding after a significant injury, is a result of a series of complex biological interactions. The coagulation time is controlled by several factors, enzymes and proteins. Coagulation time measurement provides vital information about the concentration of specific factors in blood. In this regard, various tests such as prothrombin time (PT) and activated partial thromboplastin time (aPTT) have been developed to identify amount of these specific factors. Furthermore, the blood coagulation time needs to be checked for patients who are under regular drug therapy that affects the blood viscosity [2]. Longer coagulation times may result in hemorrhage whereas too short coagulation times may result in embolism. Therefore, the dose of anticoagulant drugs administered is highly important, which is determined from the coagulation time measurements.

Typically, coagulation time measurements are performed at hospitals or medical centers, therefore, required travel is a burden for patients as well as it is not cost effective. In order to reduce the cost and improve ease of use, the disposable cartridge based patient self-testing devices have been developed [3], such as Coagu CheckXS (Roche Diagnostics) and i-STAT (Abbott Diagnostics). The operational methodology of these devices is based on electrical impedance changes. During the clotting process, ionic current passing through the blood changes, therefore, monitoring the electrical impedance demonstrates the blood coagulation time. However, this method may generate false measurements when patients use multiple drugs [4]. Therefore, these devices cannot be used especially for aged population when multiple drug use is

very common. The purpose of this section is to present a cartridge based patient self-testing method that measures blood coagulation time directly by monitoring the changing blood properties during coagulation.

In a typical arrangement, an ultrasonic transducer is coupled to a container where blood sample is contained. The transducer is excited by short electrical bursts and they can create acoustic waves in the buffer medium and in the sample as well. Acoustic reflections after reflecting from the various boundaries of the set-up reach back to the transducer where they are converted into electrical signals. In the previous studies transducers with 5 MHz [12] and 30 MHz [13] have been used. The coagulation time has been measured by monitoring the amplitude of the reflections. The relatively low operation frequency of the transducer and the fact that the transducer is not integrated with the container necessitated using large volumes of blood samples between 4 mL [14] to 40 mL [15]. This prevented previously developed ultrasonic methods to be used in portable cartridge based systems.

In this research, we demonstrate a potentially portable system that can perform coagulation time measurements using only $1\mu\text{L}$ of blood which can be easily drawn from patients fingers. To monitor coagulation time, we used high frequency (400 MHz) ultrasound transducer, which is fabricated on a quartz (glass) substrate to produce low cost cartridges. Therefore, the main advantages of the proposed device can be highlighted as miniaturized low cost cartridges and very low sample volume requirements, which make the approach suitable for patient self-testing. In the following sections, we present the cartridge geometry and the details of the piezoelectric transducer that uses a highly c-axis (002) oriented Zinc Oxide thin film. We will demonstrate the operation of the device by presenting pulse echo measurements, numerical modeling, and suggested method for tracking the resonance frequency of the transducer, for further cost and size reduction. We will show experimental results that we obtained with whole blood samples.

4.1 Materials and Methods

4.1.1 Thickness Mode Solidly Mounted Resonator (Ultrasonic Transducer)

The geometry of the cartridge is shown in Figure 13. The fused quartz plate (glass substrate) measures 1.7 cm by 2.5 cm in width and length, respectively. The thickness of the substrate is 1.2 mm and it carries the transducers on the bottom surface. It is possible to put multiple transducers on the quartz plate and provide separate electrical connections to control each transducer, which is useful to increase the accuracy and the reliability of the measurements. The fabricated quartz plate includes 5 transducers. However, in our experiments we only used a single transducer that is located at the center. Simply, the specimen of blood can be placed on the top surface of the plate such that the droplet aligns with the transducer.

Figure 14 shows the picture of the fabricated zinc oxide (ZnO) transducers on a quartz plate. The micro-fabrication process starts with patterning of electrodes on a quartz substrate. The electrodes are made of 1500 Angstrom thick gold. A ZnO film is deposited over the electrodes using magnetron sputtering technique [16]. The last step involves depositing and patterning of the second gold layer to form the ground electrode. At the end of the fabrication process, the transducers are formed at the intersections of top and bottom electrodes where ZnO film is sandwiched between those electrodes. Further information regarding the micro-fabrication process can be found in [17]. The transducers are 500 μm by 500 μm and the ZnO film thickness is 8 μm . The thin film of the piezoelectric has a highly c-axis orientation (002), therefore, the TE (Thickness Extensional) mode resonating frequency of the transducers corresponding to this geometry is equal to 400 MHz.

4.1.2 Circuitry

For pulse echo measurements, we constructed a custom system by using RF components, which their operating frequency range is between DC and 1 GHz. Figure 15A

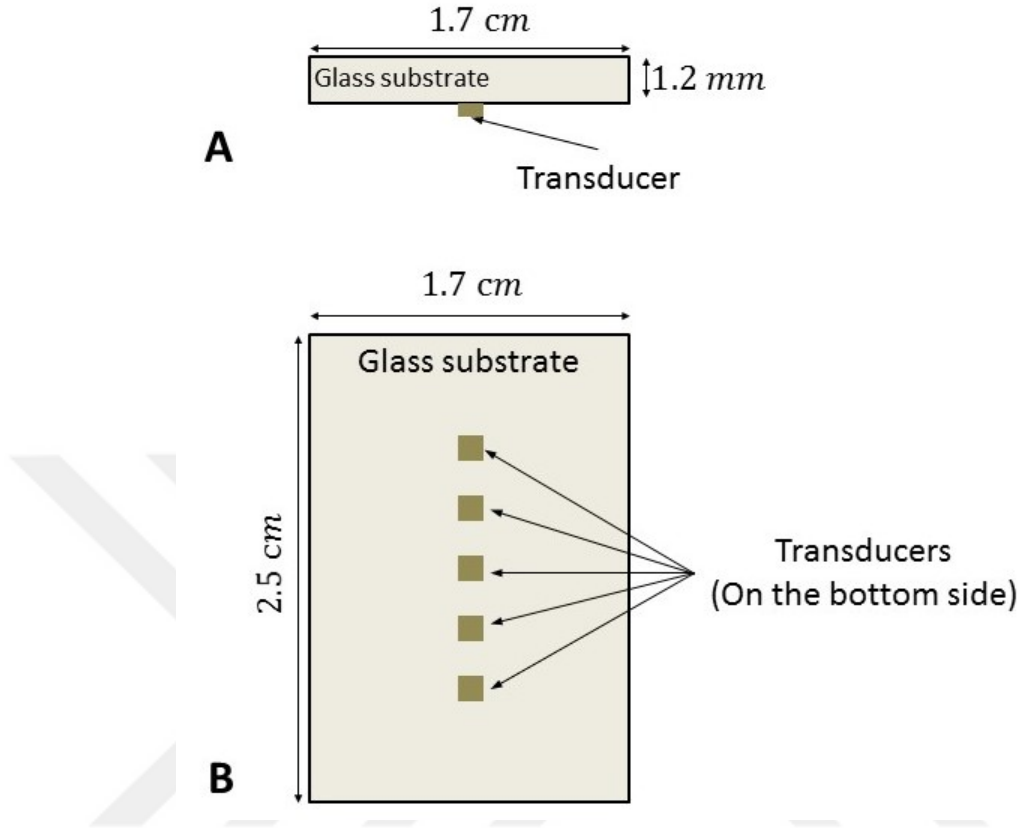


Figure 13: (A) Side view of the cartridge; (B) Top view of the cartridge. The electrical connections were not shown.

illustrates the schematic drawing of the electronics set-up with capability of pulse echo measurements. This set-up includes an arbitrary signal generator (KEYSIGHT, 81160A) that generated a burst of 400 MHz sine wave with 100 mV_{pp} at output. It also generated a TTL pulse with the same width as the sine burst to control the TTL Switch. The sinusoidal signal at the output of the signal generator was amplified using a microwave amplifier (Mini-Circuits-ZHL6+) with a gain of 20 dB. In the next stage, an SPDT (single pole double throw) TTL switch (Mini-Circuits-ZYSWA-2-50-DR) was used to direct the excitation sine burst to the transducer and reflected signals to the output amplifier (Another 20dB amplifier). To reduce the noise, a band pass filter with frequency range of 27.5 to 800 MHz was used (Mini-Circuits-BHP-25+) at the output of the second amplifier.

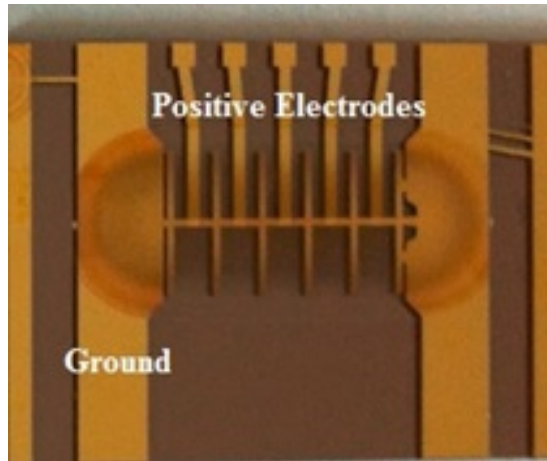


Figure 14: Bottom view of the fabricated ultrasonic transducers on the fused quartz substrate. The ground electrode is the same for all the transducers and it runs in the horizontal direction over the zinc oxide film. Other electrodes are between the zinc oxide film and the substrate.

In the experiments, we generated a burst of 14 cycles of sine waves at 400 MHz and a synchronized TTL pulse with width of approximately 50 ns with repetition rate of 1 KHz. In the transmit cycle the transducer is excited by the tone burst. In the receive cycle the transducer is connected to the 20 dB output amplifier following with the band pass filter. The output of the bandpass filter was connected to a 10 GSa/s oscilloscope (ROHDE & SCHWARZ, RTO 1014, 1 GHz Bandwidth) to collect the reflected signals coming from the transducer. The digitized data were stored on the oscilloscopes internal storage and then transferred to a personal computer for further processing.

4.1.3 The Temperature Control System

The coagulation measurements should be done at a constant temperature of human body, since the measurement temperature affects the coagulation time. Therefore, we performed all the measurements at a constant temperature of 37°Celsius. We used a temperature controlled hot plate to keep the cartridge temperature at $37\pm 0.5^\circ\text{C}$. We placed the cartridge on a hot plate and made sure that the quartz substrates

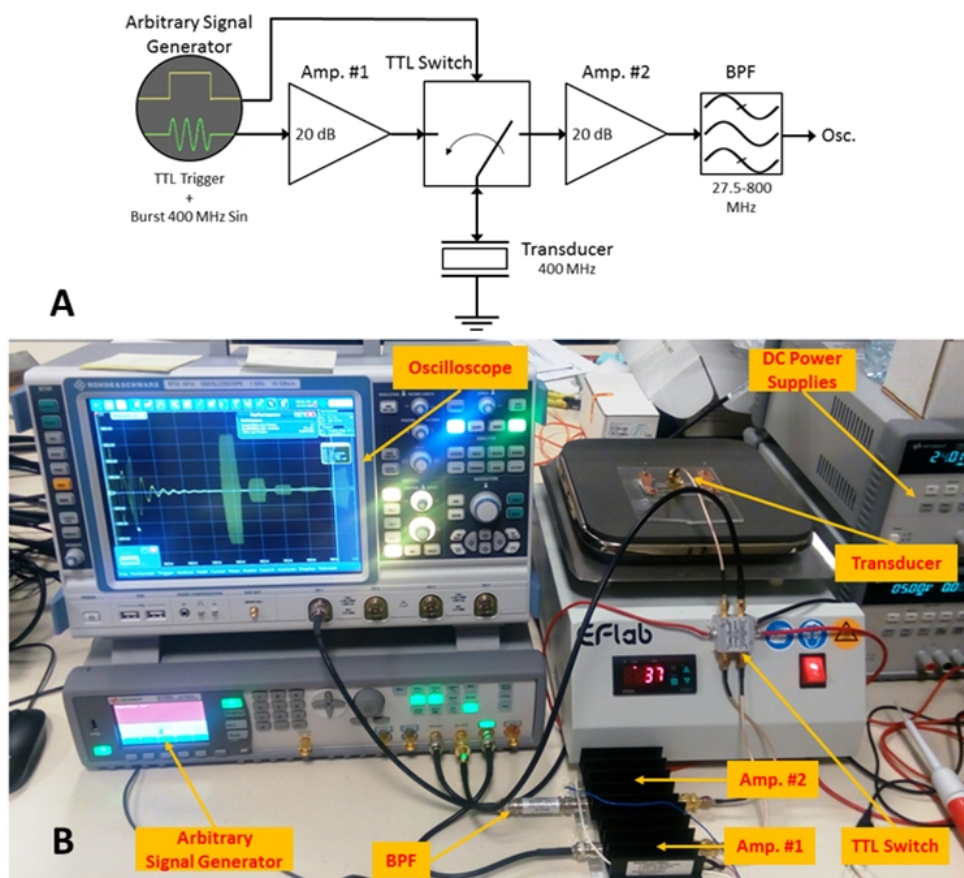


Figure 15: (A) Block diagram of the electronics set-up for pulse echo measurements; (B) A photo of the measurement set-up.

temperature has reached to 37 degrees before putting the blood sample on it. During the experiments, we also enclosed the cartridge in a small box with the hot plate. Figure 16 shows a commercially available temperature controller system from EFLAB which uses ET2011 control unit for the temperature stabilization. The blood sample and reagents were pre-heated before the experiments, by putting them also on the hot plate.

4.1.4 Pulse-Echo Measurements

We used the set-up to obtain pulse-echo measurements from the cartridge. Figure 17 demonstrates a simplified drawing of the acoustic reflections inside the cartridge. The



Figure 16: The commercial temperature control system for keeping the temperature at $37\pm 0.5^\circ\text{C}$.

transducer is excited by a short tone burst. The electrical signal is converted into the acoustic waves in the quartz substrate by the ZnO transducer. The semi-plane acoustic waves reach to the quartz-blood interface after propagating in the substrate. If there is no blood sample on the substrate, all the waves are reflected into the substrate; because of the large difference between the acoustic impedances of quartz and air. The reflected waves then arrive back to the transducer where it is converted into an electrical signal. At this point, some portion of the pulse is reflected back into the quartz substrate again. The back and forth reflections of the acoustic waves are shown in Figure 18A (Blue trace). In this figure, the first reflection is labelled R1 and the consecutive reflections are labelled R2 and R3, respectively. The thickness of the

quartz plate is approximately 1.2 mm and the longitudinal sound velocity in quartz is 5972 m/sec. By considering the total path that sound waves travel, the first pulse should arrive around 440 ns, which is in agreement with the time waveform shown in Figure 18A.

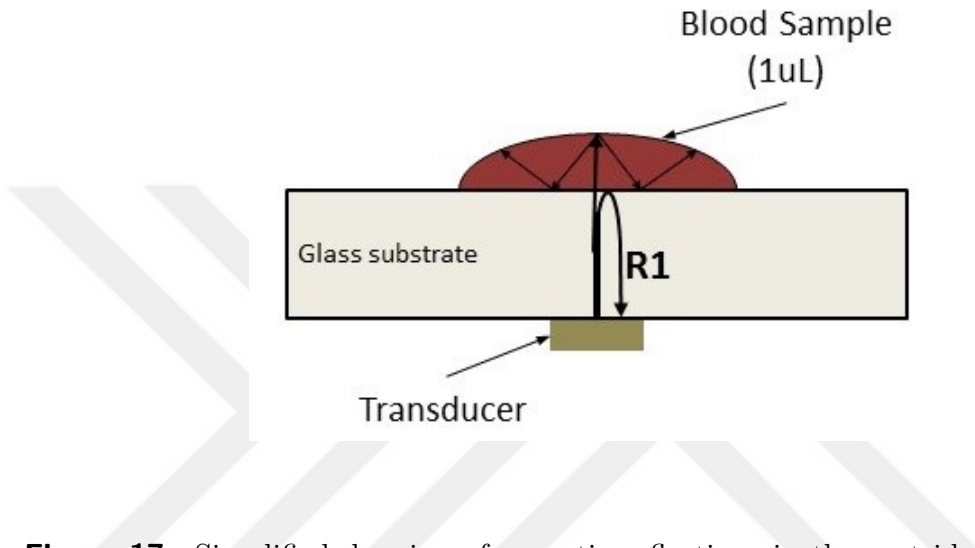


Figure 17: Simplified drawing of acoustic reflections in the cartridge, where R1 is the first reflection from boundary of the quartz substrate and the blood sample.

If a drop of liquid is placed on the substrate aligning with the location of the transducer on the other side of the cartridge, amplitudes of the R1, R2, and R3 reflections dramatically drops, due to the coupling into the liquid. In this case, some portion of the acoustic waves transmit into the liquid at the interface. The acoustic pulse propagates through the liquid and after multiple reflections, it decays out. The acoustic reflections when there is a DI water droplet on the surface is also demonstrated in Figure 18A (Red trace). As expected, the amplitudes of acoustic reflection are reduced. Figure 18B zooms around the first reflection. In this figure, we also added the reflection when there is a blood droplet on the substrate. With the blood droplet, the reflection amplitude is reduced further.

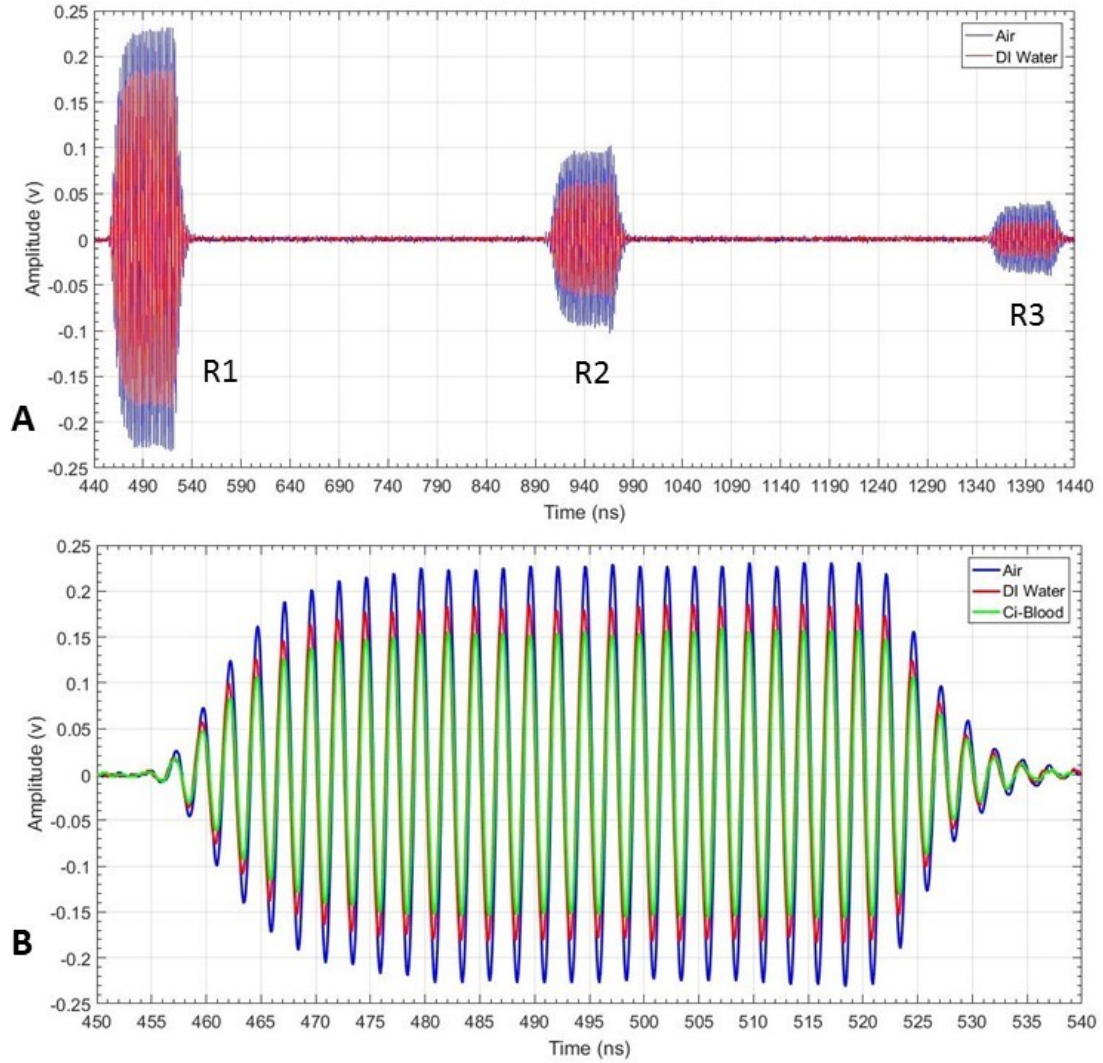


Figure 18: (A) Multiple reflections in the quartz substrate for Air and DI water; (B) The zoomed R1 pulses for Air, DI water, and Ci-Blood. The acoustic waves reflect in the quartz substrate multiple times and decay due to the acoustical and diffraction losses. Time delay between each reflection is around 440 ns which is proportional to the longitudinal sound speed (5500 m/sec) and thickness of the fused quartz (1.2 mm).

For the coagulation measurements, we only observed the RMS value of the first reflection (R1). First, we tested the stability of the system by using a drop of distilled

water. Figure 19 presents the RMS value for the first reflection (R1) amplitude over 480 sec. For this measurement, oscilloscope traces were acquired at every 10ms and stored in a computer. Then, RMS amplitude of R1 was calculated over a 40 ns window around R1 reflection (16 cycles of sine waves) between 470 ns to 510 ns. The slight drift at the beginning on the curve is due to the temperature equalization of the distilled water. In the next sections, we demonstrate the dependency of the R1 amplitude with quartz/liquid reflection coefficient and summarize the results we obtained from whole blood samples.

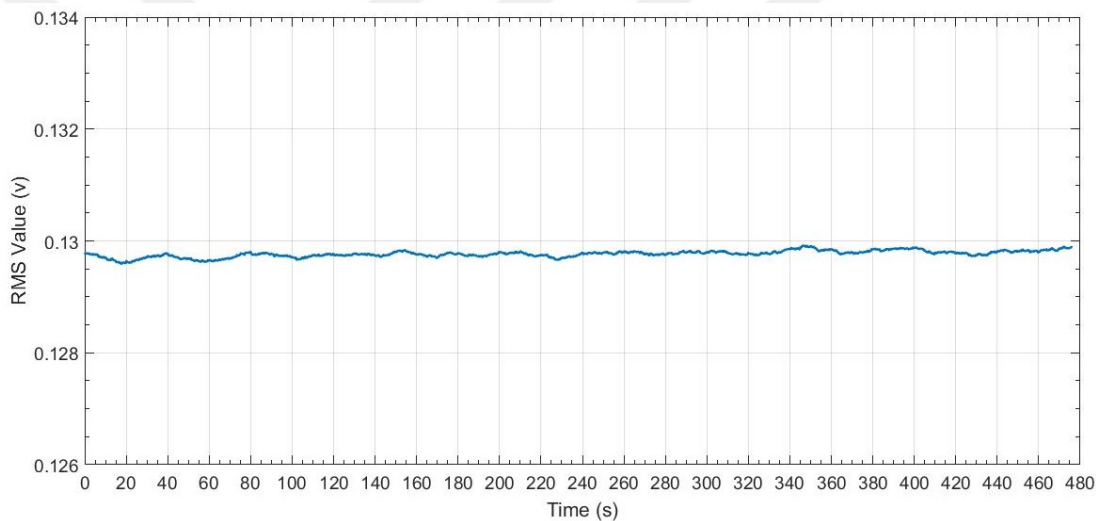


Figure 19: The computed RMS value of reflected R1 pulse, while a drop of DI water was put on the quartz substrate.

4.1.5 Blood Sample Preparation

Human blood samples were drawn from a healthy 27 year old person under the Ozyegin University Ethical Committees approval and the volunteers signed informed consent. The blood samples were stored in an evacuated 2 mL blood tube with 3.2 percentage of citrate (9NC %3.2). For all the experiments, fresh blood samples of less than two hours old were used. We functionalized the cartridge surface with CaCl₂. For this purpose, we put 1 μ L of 20 mM CaCl₂ solution on the substrate and let the

substrate to reach 37 degrees Celsius. Then, we waited until all the water evaporates. Before coagulation experiments, we also heated the blood and reagent solution for 2 minutes at 37 degrees Celsius.

For the aPTT time measurements, after preheating, 20 μL of blood samples were mixed with 20 μL of aPTT reagent solution (SynthASil) for 5 minutes which is the specified incubation time for the aPTT reagent. Then, 1 μL of the mixture solution was put on the dried CaCl_2 on the substrate and simultaneously the oscilloscope was started to collect the reflection data with repetition period of 10 ms. The functionalized substrate with CaCl_2 was used only for the tests when CaCl_2 needed to be added to the mixture. For other tests, a substrate without CaCl_2 was used. To demonstrate the capability of the proposed measurement method, the coagulation times for two different mixtures of Heparin and blood were also used.

4.1.6 Numerical Modeling of th Acoustic Waves Propagation

A simplified numerical modeling was done to show longitudinal wave propagation inside the materials and amplitude dependency to the reflection coefficient of the quartz/liquid boundary. Figure 20 illustrates the simplified electrical modeling of the cartridge. Each part of the cartridge and the mediums were modeled as electrical waveguides with specific acoustic properties such as length, speed of sound, and acoustic impedance. In operation, the transducer produces compressional and tensional pressures on the both sides, where attached to the gold electrodes. Therefore, these type of pressure vibrations of the transducer is modeled as two pressure sources in opposite direction. In other hands, the effect of the gold electrodes was ignored on the acoustical wave propagations, where their thicknesses are much smaller than the wavelength at 400MHz. The AC voltage sources in Figure 20, generate 14 cycles of sinusoidal waves during the excitation at time equals to zero, and become short circuits for the rest of the time. Likewise, for capturing the reflected acoustics, the

voltages (pressures) on the both sides of the transducer are measured versus the time. All these numerical calculations were done using MATLAB, somehow to capture 3 consecutive reflections of the acoustic waves from quartz/liquid boundary. This gave us opportunity to compare the numerical results with practical measurements.

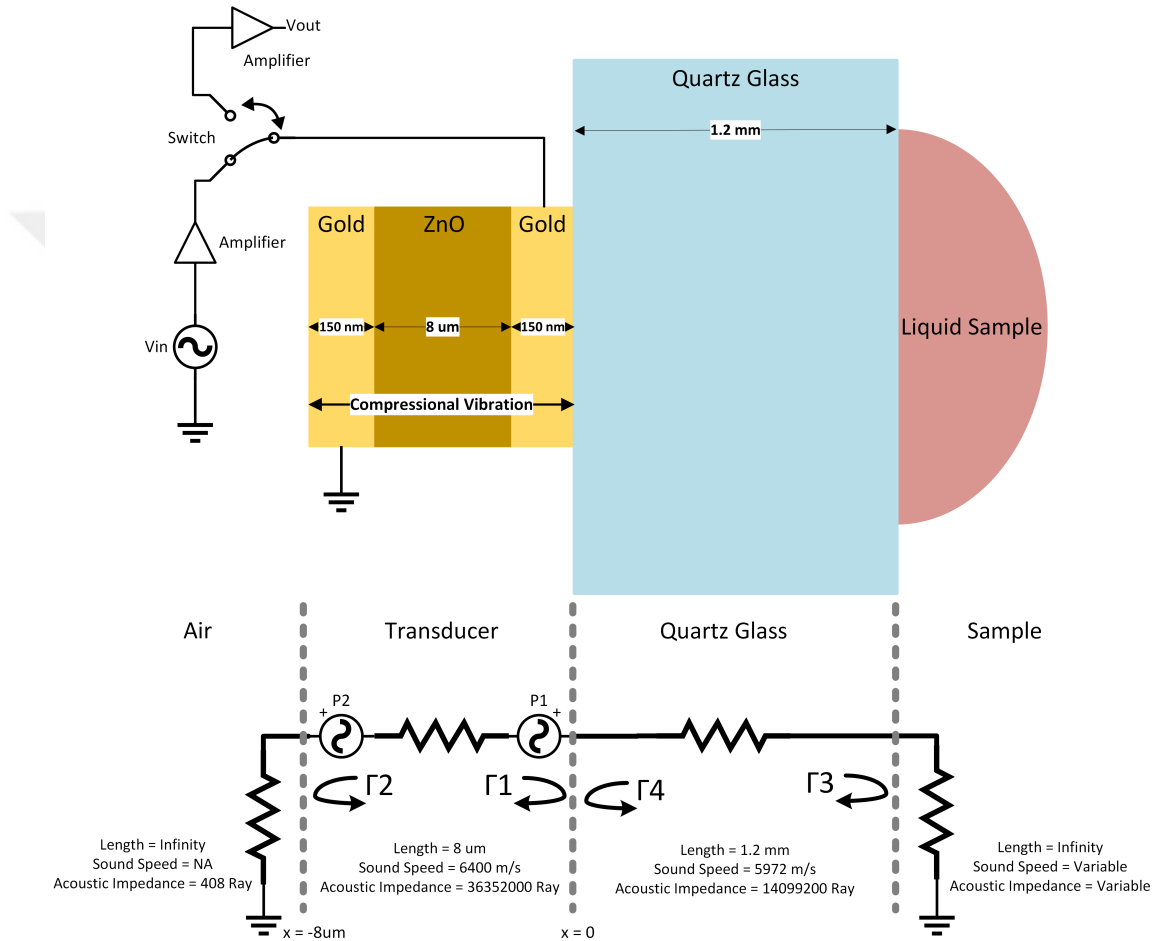


Figure 20: The simplified modeling of the proposed disposable cartridge and liquid sample. The compressional vibration of the transducer is modeled as two mechanical pressure in opposite direction.

Equation (1) models the relation between input electrical voltage and excitation pressures on both sides of the transducer, where K_{in}, G_{in} are the transducer input electrical to mechanical coupling factor, and input amplifier gain, respectively.

Equations (2) and (3) are the excitation pressures caused by input voltage of $V_{in}(t)$ where the $L_T, C_T, \Gamma_1, \Gamma_2, \Gamma_3, \Gamma_4$ are the transducer length, speed of sound in transducer (ZnO), Quartz/Zno reflection coefficient ($\simeq -0.4411$), Air/Zno reflection coefficient ($\simeq -1$), Sample/Quartz reflection coefficient (variable), and Zno/Quartz reflection coefficient ($\simeq 0.4411$), respectively. The total pressure on the transducer is summation of these two pressures.

$$P_{exc.1}(t) = P_{exc.2}(t) = \frac{V_{in}(t)}{2} \times K_{in} \times G_{in} \times \sin(2\pi ft) \times \left[u(t) - u\left(t - \frac{N_{Cycles}}{f}\right) \right] \quad (1)$$

$$P_{x=0, \#1}(t) = \left\{ \sum_{i=0,1,\dots}^{\infty} \left[P_{exc.1}\left(t - 2i \frac{L_T}{C_T}\right) \times (\Gamma_2^i \times \Gamma_1^i \times (1 - |\Gamma_1|)) \right] \right\} + \left\{ \sum_{i=0,1,\dots}^{\infty} \left[P_{exc.2}\left(t - (2i + 1) \frac{L_T}{C_T}\right) \times (\Gamma_2^{i+1} \times \Gamma_1^i \times (1 - |\Gamma_1|)) \right] \right\} \quad (2)$$

$$P_{x=-sum, \#1}(t) = \left\{ \sum_{i=0,1,\dots}^{\infty} \left[P_{exc.2}\left(t - 2i \frac{L_T}{C_T}\right) \times (\Gamma_2^i \times \Gamma_1^i \times (1 - |\Gamma_2|)) \right] \right\} + \left\{ \sum_{i=0,1,\dots}^{\infty} \left[P_{exc.1}\left(t - (2i + 1) \frac{L_T}{C_T}\right) \times (\Gamma_1^{i+1} \times \Gamma_2^i \times (1 - |\Gamma_2|)) \right] \right\} \quad (3)$$

Equations (4), (7), and (10) show the first, second, and third acoustic wave reflections coming back from Sample/Quartz boundary towards the transducer, respectively. In these equations, α, L_Q, C_Q are indicating the loss coefficient, quartz length, and speed of sound in quartz, respectively. The captured pressure on both side of the transducer due to the first, second, and third reflections are illustrated in Equations (5), (6), Equations (8), (9), and Equations (11), (12), respectively. Because the reflection waves decay gradually due to the reflection and transmission losses, therefore only 6 iterations were used for all the series, where the absolute infinity was indicated.

$$P_{reflection, \#1}(t) = (1 - 2\alpha) \times P_{x=0, \#1} \left(t - 2 \frac{L_Q}{C_Q} \right) \times (\Gamma_3 \times (1 - |\Gamma_4|)) \quad (4)$$

$$P_{x=0, \#2}(t) = \sum_{i=1,2,\dots}^{\infty} \left[P_{reflection, \#1} \left(t - 2i \frac{L_T}{C_T} \right) \times (\Gamma_2^i \times \Gamma_1^{i-1} \times (1 - |\Gamma_1|)) \right] \quad (5)$$

$$P_{x=-8um, \#2}(t) = \sum_{i=0,1,\dots}^{\infty} \left[P_{reflection, \#1} \left(t - (2i + 1) \frac{L_T}{C_T} \right) \times (\Gamma_1^i \times \Gamma_2^i \times (1 - |\Gamma_2|)) \right] \quad (6)$$

$$P_{reflection, \#2}(t) = (1 - 2\alpha) \times P_{x=0, \#2} \left(t - 2 \frac{L_Q}{C_Q} \right) \times (\Gamma_3 \times (1 - |\Gamma_4|)) \quad (7)$$

$$P_{x=0, \#3}(t) = \sum_{i=1,2,\dots}^{\infty} \left[P_{reflection, \#2} \left(t - 2i \frac{L_T}{C_T} \right) \times (\Gamma_2^i \times \Gamma_1^{i-1} \times (1 - |\Gamma_1|)) \right] \quad (8)$$

$$P_{x=-8um, \#3}(t) = \sum_{i=0,1,\dots}^{\infty} \left[P_{reflection, \#2} \left(t - (2i + 1) \frac{L_T}{C_T} \right) \times (\Gamma_1^i \times \Gamma_2^i \times (1 - |\Gamma_2|)) \right] \quad (9)$$

$$P_{reflection, \#3}(t) = (1 - 2\alpha) \times P_{x=0, \#3} \left(t - 2 \frac{L_Q}{C_Q} \right) \times (\Gamma_3 \times (1 - |\Gamma_4|)) \quad (10)$$

$$P_{x=0, \#4}(t) = \sum_{i=1,2,\dots}^{\infty} \left[P_{reflection, \#3} \left(t - 2i \frac{L_T}{C_T} \right) \times (\Gamma_2^i \times \Gamma_1^{i-1} \times (1 - |\Gamma_1|)) \right] \quad (11)$$

$$P_{x=-8um, \#4}(t) = \sum_{i=0,1,\dots}^{\infty} \left[P_{reflection, \#3} \left(t - (2i + 1) \frac{L_T}{C_T} \right) \times (\Gamma_1^i \times \Gamma_2^i \times (1 - |\Gamma_2|)) \right] \quad (12)$$

The total sensed pressures and voltages on the transducer due to these three consecutive reflections can be calculated by Equations (13) and (14), where K_{out} and G_{out} are the transducer output mechanical to electrical coupling factor, and output amplifier gain, respectively. By substituting the amplifier gains as 10 (20dB), and Sample/Quartz reflection coefficient as -0.9999 by considering the air as the sample, the rest of the unknown values were calculated numerically to fit the numerical modeling curve on the practical measurement curve as much as possible as shown in Figure 21. These calculations yielded the output voltage is directly depended to the Sample/Quartz reflection coefficient. Therefore, the output voltage of the first reflection can be calculated from Equations (15) and (16).

$$P_{Out}(t) = \sum_{i=1}^4 P_{x=0, \#i}(t) + \sum_{i=1}^4 P_{x=-8um, \#i}(t) \quad (13)$$

$$V_{Out}(t) = K_{out} \times G_{out} \times \left\{ \sum_{i=1}^4 P_{x=0, \#i}(t) + \sum_{i=1}^4 P_{x=-8um, \#i}(t) \right\} \quad (14)$$

$$|V_{Out}(t)| \approx 0.22714 \times |\Gamma_3| \quad (15)$$

$$\Gamma_3 = \frac{Z_{liquid} - Z_{quartz}}{Z_{liquid} + Z_{quartz}} \quad (16)$$

The amplitude of first reflection for multiple practical measurements were compared with the numerical modeling results obtained by Equations (15) and (16) for two different samples of air and distilled water. The maximum errors obtained for the air and distilled water are 1.76% and 1.24% respectively. The small value of errors indicates how the numerical modeling good describes the practical behavior of the output voltage versus the sample. Thus, these results motivated us to concentrate on measuring the amplitude of the first reflections for real blood testing and make sure any changes on the RMS value is directly related to the blood (sample) properties.

4.1.7 Mason Modeling and Resonance Frequency

Although the practical measurements were done based on the pulse-echo method and data acquisition for a short burst of 400MHz signals, but a Mason modeling also was done to show dependency of resonance frequency to the blood (or water) sample. This method of measurements can be considered as an alternative way, where the required electronic unit can be further simplified and ended up with a smaller and more cheaper device.

As described in previous chapter, the proposed transducer can be considered as a multiple acoustic layers. The acoustic impedance seen from both side of the transducer can be implemented into the input impedance equation of the transducer. The complex input impedance of the transducer provides invaluable information of the transducer regarding the resonance frequency, quality factor, bandwidth, and etc.

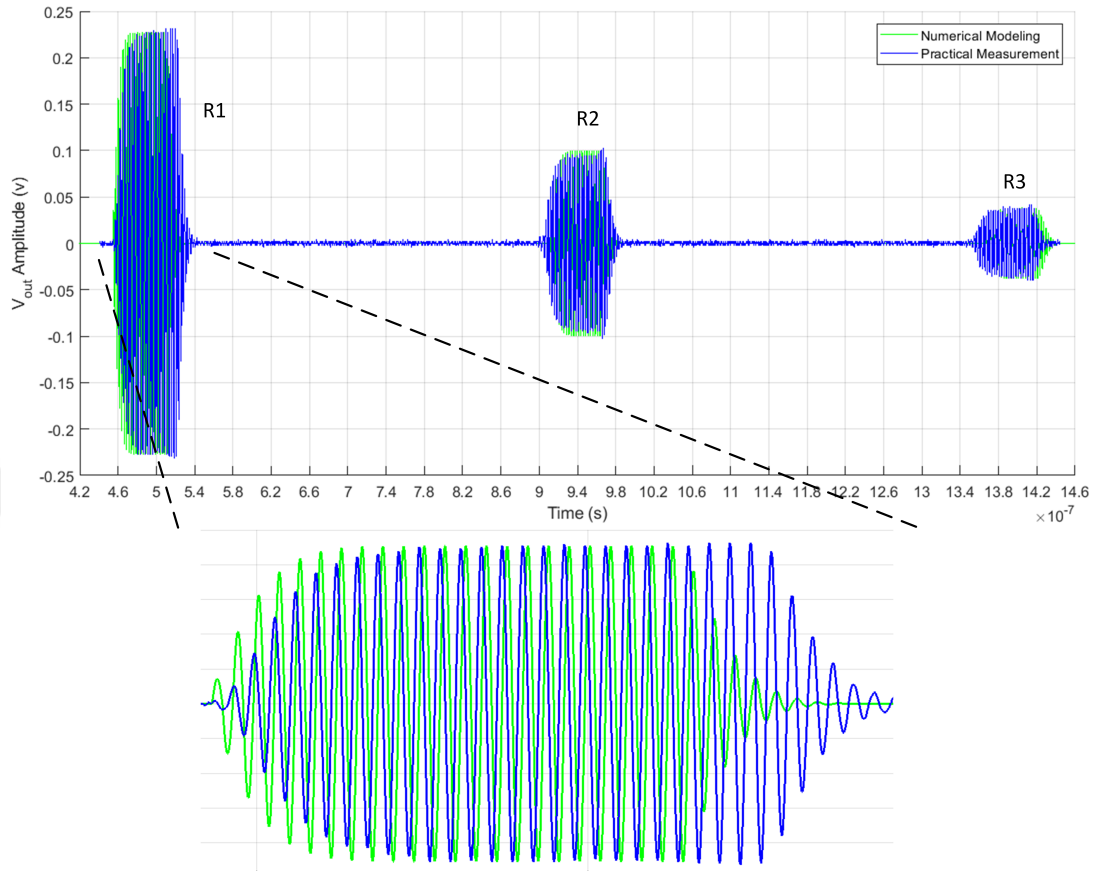


Figure 21: Comparison of the practical measurement versus the numerical modeling, when there is no liquid on the quartz (medium is air). The amplitude for the both practical and modeling results are almost same along the three reflections.

Based on these information, the transducer and liquid sample can be modeled with inductor and resistor which is a good feedback of the transducer design or a start point of the fabrication optimizations.

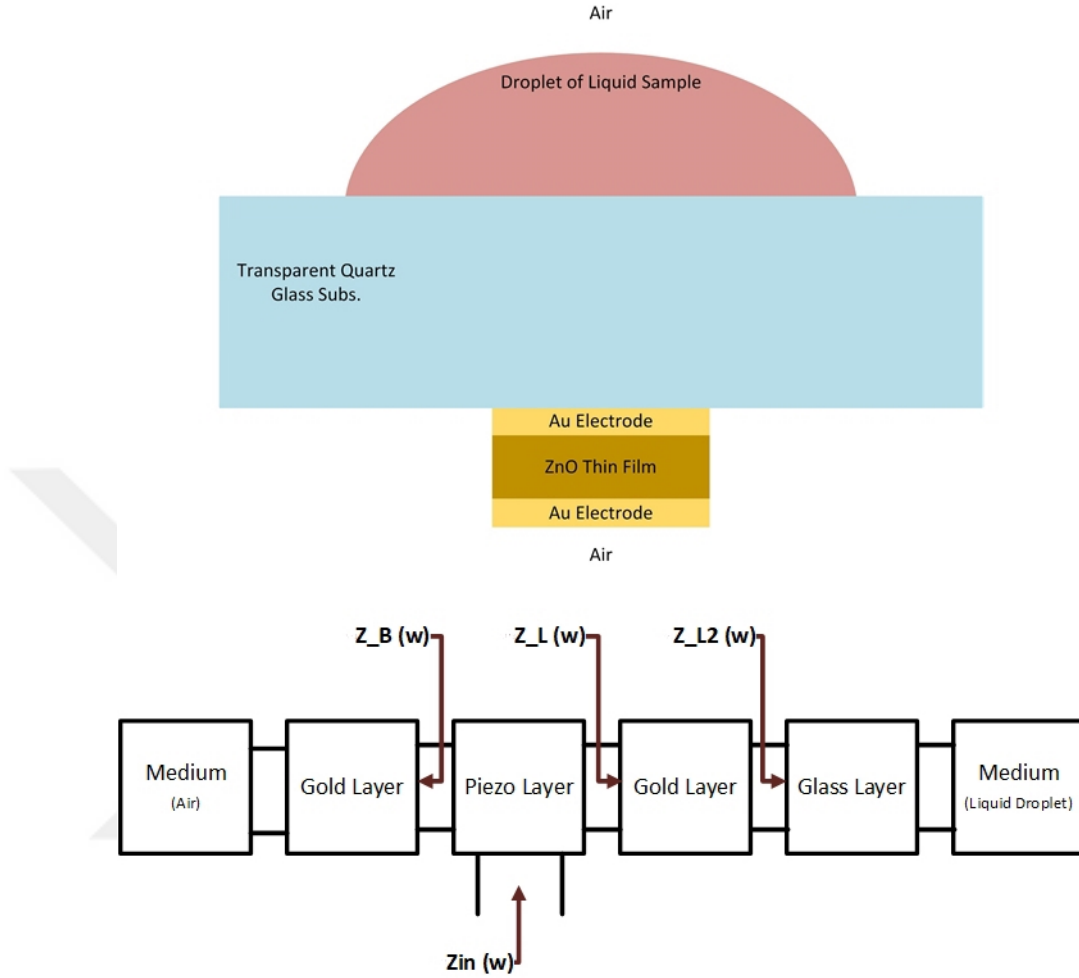


Figure 22: The transducer and mediums as acoustical layers.

Figure 22 demonstrates the transducer's acoustical layers. $Z_{in}(\omega)$ is the complex input impedance seen from transducer. The mechanical impedance for liquid and air mediums can be derived from equations (17) by using the parameters provided in table (1), where the ρ , μ , κ , v_L , λ , μ_B , and α are density, shear viscosity, adiabatic compressibility, compressional sound speed, second viscosity, bulk viscosity, and attenuation factor, respectively.

Table 1: Mechanical and acoustical properties of water, whole blood, and air.

Material	ρ (kg/m ³)	μ (Pa. s)	κ (GPa ⁻¹)	v_l (m/s)	Thickness (m)
Water @ 23°	998	0.89e-3	0.455	1489	Inf.
Air	1.204	0.1813e-4	7047	343.3	Inf.
Whole Blood	1055	3.5e-3	0.38	1580	Inf.

$$v_l = \sqrt{\frac{cE_{33}}{\rho}} \quad \text{for solids}$$

$$Z = R + jX = \sqrt{\rho[\rho v_l^2 + j\omega(2\mu + \lambda)]}$$

$$\mu_B = \frac{2}{3}\mu + \lambda \quad (17)$$

$$\alpha = \alpha_{Np} \cong \frac{2\omega^2 \kappa \mu}{3v_l}$$

$$R = \frac{\rho v_l \omega^2}{\omega^2 + \alpha^2 v_l^2}, \quad X = \frac{\rho v_l^2 \omega \alpha}{\omega^2 + \alpha^2 v_l^2}$$

Numerical calculations and modeling were done in Matlab. Absolute value and phase of complex input impedance are illustrated in Figure 23 and 24, respectively, for three different sample droplets (mediums). As expected, the quality factor where the air is much greater than whole blood and water. This comes from huge impedance mismatches in quartz/medium interface, which traps more acoustic energy inside the bulk thin film. The lowest impedance peak relates to the resonance frequency where the maximum displacement of the piezo thin film in thickness mode is desired. Figure 25 illustrates an eigenfrequency analysis of the device simulated in COMSOL; the maximum TE mode displacement (resonance) occurs at 400 MHz, as expected.

Figure 26 illustrates the three resonance frequency of the transducer with space of roughly 2.4 MHz which correspond to the resonance of glass substrate. In practice, we chose the 400MHz excitation sine wave because of its higher amplitude that we captured. Other resonance frequencies usually have lower effect because of the attenuation of the acoustic layers. Therefore, for the rest of the simulations and numerical calculations, we considered 400MHz as a fundamental resonance frequency of the transducer.

Table 2: Some properties of used materials in simulation and calculations.

Material	ρ (kg/m ³)	c_{33} (G Pa)	e_{33} (C/m ²)	ϵ_{33}^S (F/m)	v_l (m/s)	Z_0 (M Ray)	Thickness (m)
Zinc Oxide	5700	211	1.32	8.85e-11	6361.7	36.262	8e-6
Gold	19300	70	-	-	1904.5	36.76	150e-9
Quartz (Glass)	2203	73.1	-	-	5760.4	12.69	1.2e-3

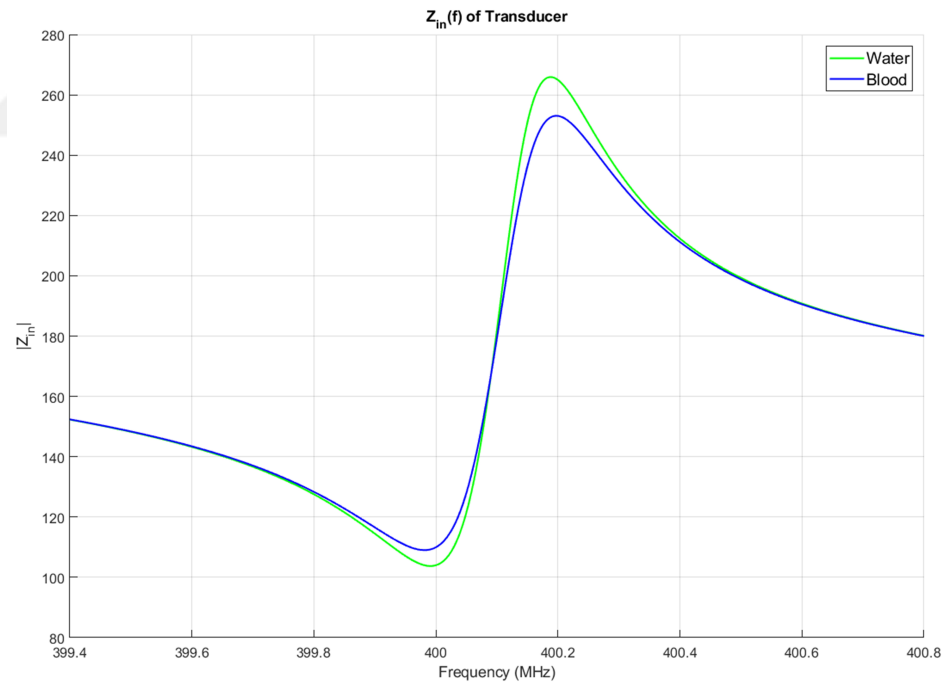
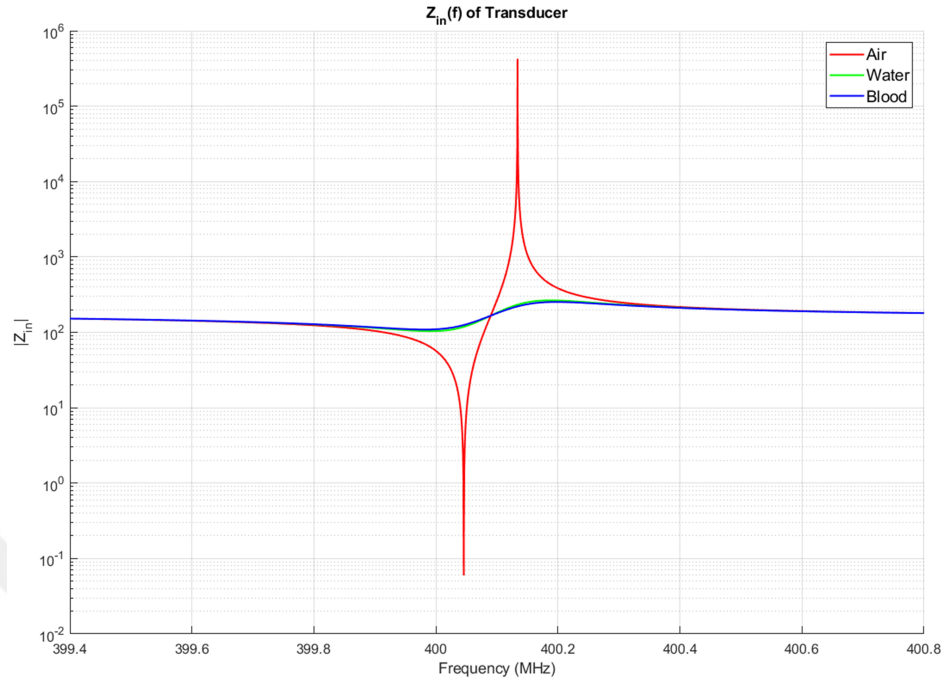


Figure 23: Absolute value of input impedance versus frequency.

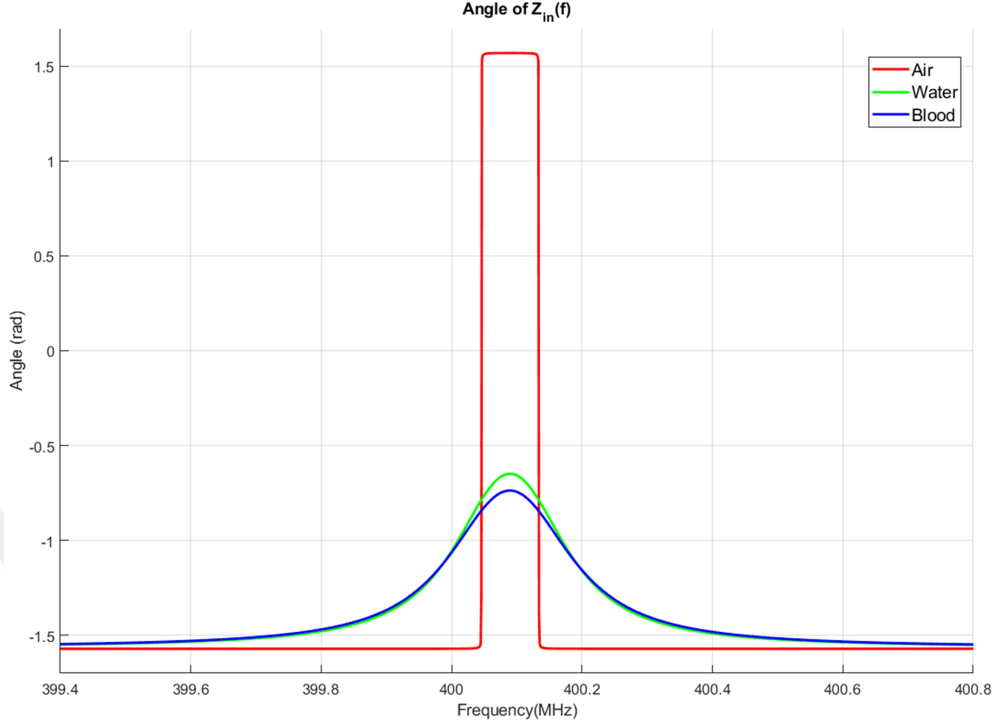


Figure 24: Phase of input impedance versus frequency.

Based on the simulations and numerical calculations, quality factor of the resonator reversely related and bandwidth of the transducer directly related to the amplitude value of the medium impedance. Figure 27 illustrates the F_s (series/resonance frequency), F_p (parallel/anti-resonance frequency), and Q_s (quality factor of series/resonance frequency) for three different sample droplets (medium). The droplet was considered to have infinity thickness, so the acoustic waves propagating inside the medium can not be reflected back. Mason modeling of the input impedance shows effect of sample's impedance on the resonating parameters. This possibility can be used as an alternative way to measure the blood coagulation time measurement just by tracking the resonance frequency and quality factor. Since the Mason modeling provides a complex input impedance, therefore the effect of complex sample can also be analyzed for viscosity measurements; specially for an expensive drugs or chemicals which the lower testing volume is required. The readout circuitry can be designed and fabricated with

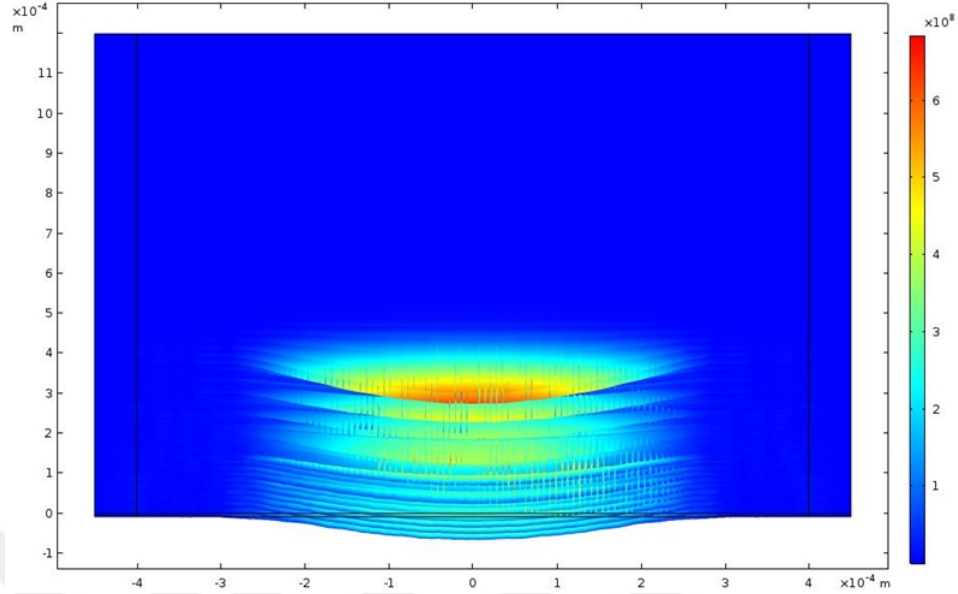


Figure 25: Maximum TE displacement of the transducer at resonance frequency, simulated in COMSOL.

a simple asymmetric oscillator and digital counter on the same substrate.

4.1.8 Results and Discussions

The method was tested first with citrated blood. In this way, 1 mL of the citrated blood was put on the substrate using an auto pipette following the procedure explained in the previous section. In this experiment, the substrate was not functionalized with CaCl_2 . The RMS value of the R1 amplitude for citrated blood is demonstrated in Figure 28 (red curve). The total noise of the measurement system is around 25 mVRMS. We hypothesize that the fluctuations in the measurement for citrated blood are due to the slow sedimentation of the red blood cells. For this experiment, we did not observe any sudden change of the amplitude. This indicates the citrated blood did not coagulate on the substrate. We also observed citrated blood in a small container and as expected the blood did not coagulate over 10 minutes. We also fitted a curve using a polynomial fit algorithm. Later we used the fitted curves to calculate the derivative of the measurement. Our polynomial fit algorithm chooses

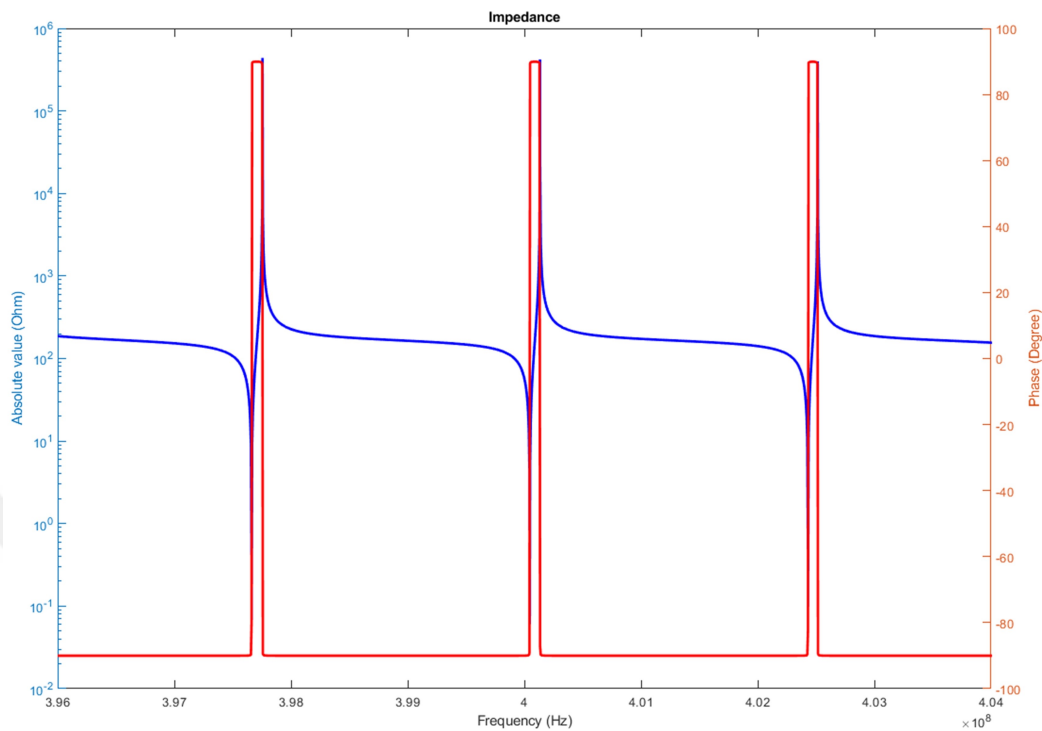


Figure 26: Absolute value and phase of Input impedance of the transducer for multiple resonance frequencies without considering the loss effect.

the minimum polynomial order that results in the best fit that minimizes the error between the actual data and the fitted curve.

In the second experiment, we used the functionalized surface of the cartridge (CaCl₂ on the substrate) and placed 1 μ L of blood with aPPT reagent on the surface. We obtained the green curves shown in Figure 28. The dashed curve is the polynomial fit to the actual measurement data. We used the maximum of the first derivative to obtain the coagulation time as described in [9].

Figure 28 also shows aPTT measurements for two different concentrations of heparin solutions mixed with blood. All 4 experiments described in Figure 28 repeated 5 times. Only one curve from each set of 5 curves was included in Figure 28. Figure 29 summarizes all the measurements that we obtained using the described method. As expected, the coagulation time increases while the heparin content increased. The average coagulation times for multiple aPTT measurements are 24.93, 32.75, and 46.75

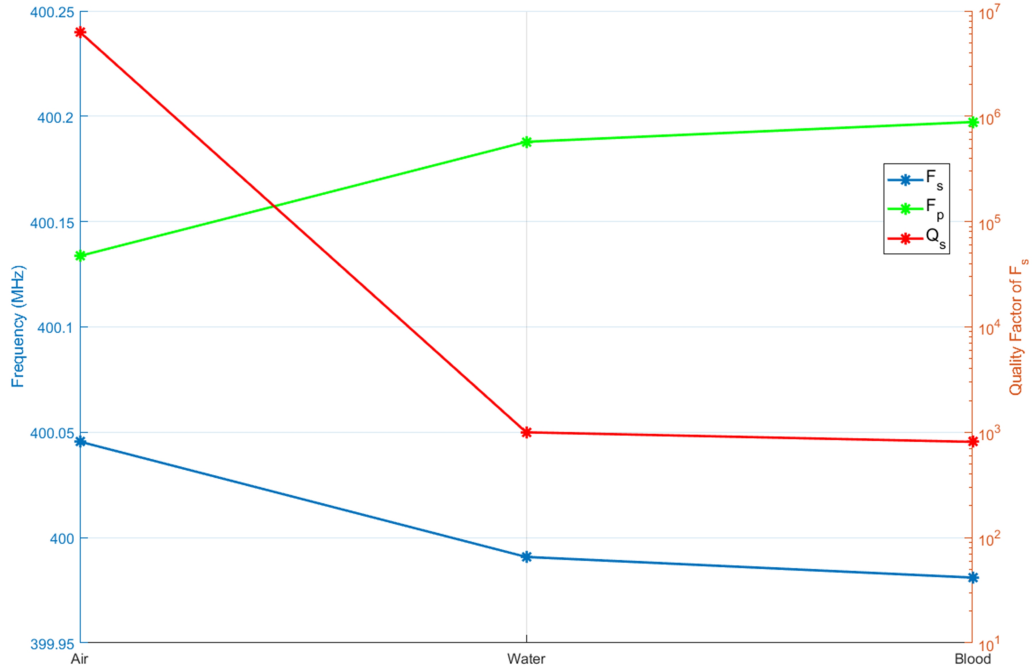


Figure 27: Comparison of resonance frequency and quality factor for three different droplet samples.

sec. for the blood heparin mixtures of 0.0%, 3.3%, and 6.7% volume of Heparin, respectively. Furthermore, the coagulation time in absence of heparin was found to be around 25 seconds which is in agreement with the aPTT reagents standard (SynthASil 0020006800 - Datasheet).

Above experiments reveal the potential of the method for patient self-testing. In the actual implementation, there is no need for the dried calcium agent on the cartridge since the blood will come from a finger prick rather than a citrated tube. But, the surface of the cartridge should be covered by the appropriate reagents depending on the type of the test. Multiple transducers allow multiple measurements on the same cartridge. For example, two transducers can be used for aPTT and PT measurements whereas the third one can be used for control purposes with or without any reagents. In the experiments, we directly placed a drop over the surface. However, in the actual implementation a well micro-reservoir can be fabricated over

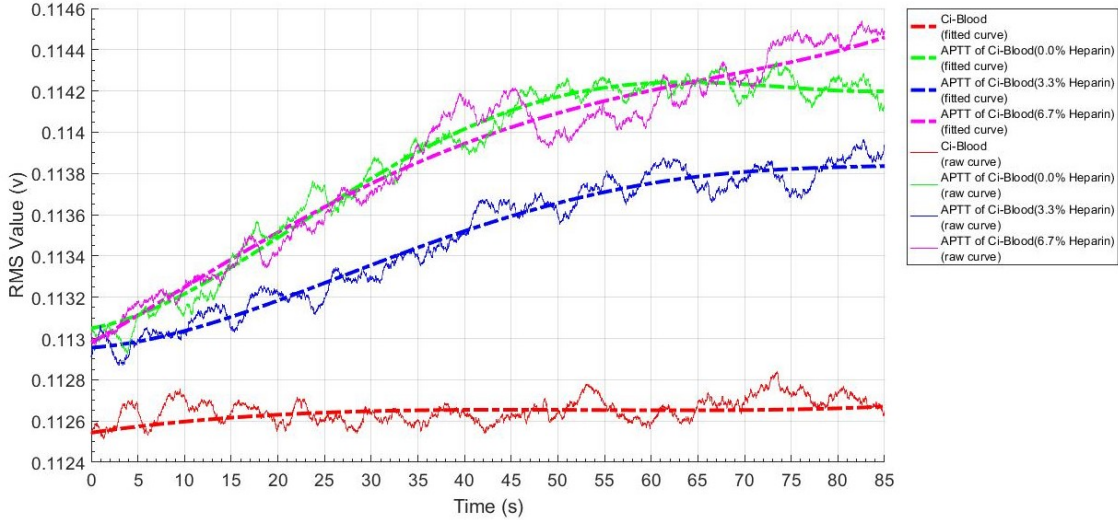


Figure 28: The calculated RMS value of raw and fitted curves of R1 for aPTT tests. Only one set was shown in this figure. We repeated each test 5 times. As heparin volume increases in the blood mixtures, settling time (or coagulation time) also increases.

the transducer. The micro-reservoir can be filled with dried reagent. Similarly, it is possible to use a fluidic channel in order to carry blood into desired locations. In the experiments, we mixed the blood with reagents using an auto pipette, in the actual implementation one can use transducers to acoustically mix the blood with the dried reagents on the surface. Previously, ultrasound had been used to perform mixing in the microfluidic channels. As described in the earlier works [17,18] one can use radiation pressure to mix the blood with reagents on the substrate. This should increase the repeatability and reliability of the tests since the red blood cell sedimentation will be prevented as well as reagents will be mixed with blood uniformly. In this work, we have used expensive off the shelf instruments. Although, the electronics for a short burst excitation and readout are relatively simple and can be constructed at a very low cost by using electronics components that work at the specified frequencies to build a low-cost reader unit, but an alternative way could be using an oscillator to track the resonance frequency instead of the time analysis. This will further reduce

the cost and size of the unit.

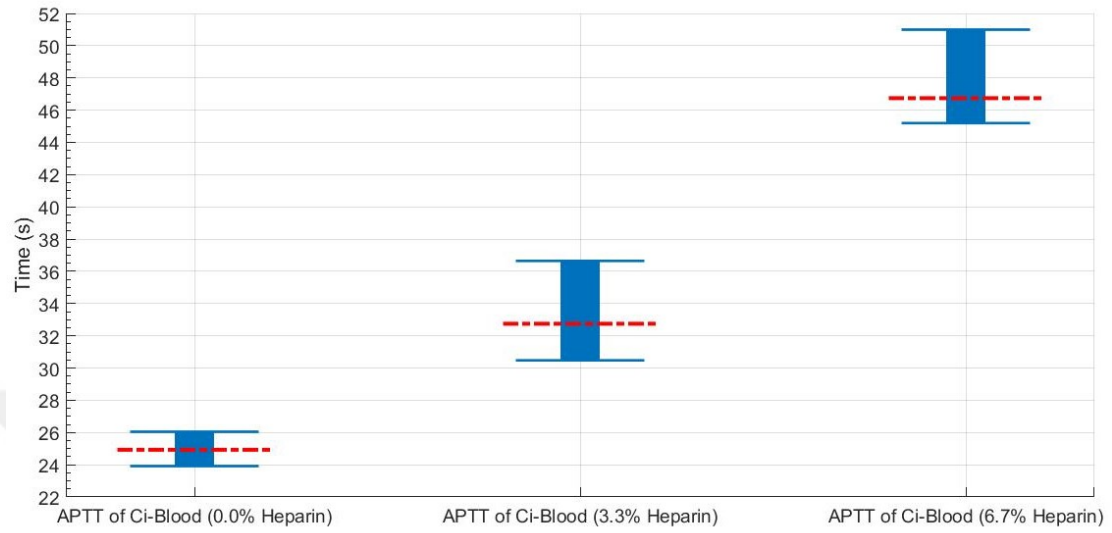


Figure 29: The computed coagulation time measurement based on the average, minimum, and maximum values for three different concentrations of blood and heparin mixtures.

CHAPTER V

CONCLUSION

In this thesis, we have demonstrated blood coagulation time measurement using a high frequency ultrasound transducer utilizing longitudinal by using a drop of whole blood sample on a quartz substrate where a transducer is placed on the other surface. The method requires only 1 %L of whole blood which makes the proposed methodology much more patient friendly compared to the existing systems which typically require 5 to 10 %L of blood. The low volume requirement of blood is achieved by using high frequency ultrasonic waves. The piezoelectric film thickness and the operation frequency are inversely proportional. Therefore, high frequency operation also reduces the cartridge cost by requiring a piezoelectric thin film which can be built by a short deposition time. Overall the cartridge cost is relatively low since it uses low cost materials and requires simple MEMS fabrication techniques.

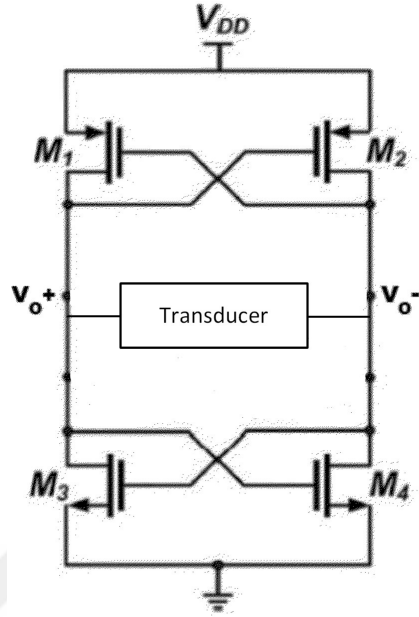


Figure 30: Asymmetric oscillator circuit.

In this thesis, we demonstrated two possible methods for blood coagulation time measurement. First one is based on the amplitude of the reflected acoustic waves from boundary of the quartz and blood sample. This method requires a short burst of 400MHz signal excitation and data acquisition versus the time. The measurements and simulations were shown for this method. The second method, could be using a simple oscillator with digital counter which tracks the resonance frequency of the transducer versus the time. The simulation for this method was presented to show sensitivity and dependency of the resonator parameters for the proposed thickness mode solidly mounted bulk acoustic resonator. A simple circuitry can be used for this purpose as illustrated in Figure 30. This method may result in further cost and size reduction as required much simpler electronic circuitry. The electronic unit can be fabricated on the same substrate if a CMOS compatible piezoelectric is considered as the transducer material, like AlN.

- [1] Bartlett, Stewart Gavin, and Paul James Hirschausen. "Apparatus and method for medical scanning." U.S. Patent Application 12/675,473.
- [2] Lison, S.; Spannagl, M. Monitoring of direct anticoagulants. *Wiener Medizinische Wochenschrift* 2011, 161, 5862, doi:10.1007/s10354-011-0876-8.
- [3] Malhotra, B. D.; Chaubey, A. Biosensors for clinical diagnostics industry. *Sensors Actuators B Chem.* 2003, 91, 117127, doi:10.1016/S0925-4005(03)00075-3.
- [4] Barcellona, D.; Fenu, L.; Cornacchini, S.; Marongiu, F. Point-of-care (POCT) prothrombin time monitors: is a periodical control of their performance useful? *Thromb. Res.* 2009, 123, 775779, doi:10.1016/j.thromres.2008.08.006.
- [5] Faivre, M.; Peltie, P.; Planat-Chretien, A.; Cosnier, M.-L.; Cubizolles, M.; Nougier, C.; Negrier, C.; Pouteau, P. Coagulation dynamics of a blood sample by multiple scattering analysis. *J. Biomed. Opt.* 2011, 16, 57001, doi:10.1117/1.3573813.
- [6] Tripathi, M. M.; Hajjarian, Z.; Van Cott, E. M.; Nadkarni, S. K. Assessing blood coagulation status with laser speckle rheology. *Biomed. Opt. Express* 2014, 5, 817, doi:10.1364/BOE.5.000817.
- [7] Ramaswamy, B.; Yeh, Y.-T. T.; Zheng, S.-Y. Microfluidic device and system for point-of-care blood coagulation measurement based on electrical impedance sensing. *Sensors Actuators B Chem.* 2013, 180, 2127, doi:10.1016/j.snb.2011.11.031.
- [8] Puckett, L. G.; Barrett, G.; Kouzoudis, D.; Grimes, C.; Bachas, L. G. Monitoring blood coagulation with magnetoelastic sensors. *Biosens. Bioelectron.* 2003, 18, 67581, doi:10.1016/S0956-5663(03)00033-2.
- [9] Cakmak, O.; Ermek, E.; Kilinc, N.; Bulut, S.; Baris, I.; Kavakli, I. H.; Yaralioglu, G. G.; Urey, H. A cartridge based sensor array platform for multiple coagulation measurements from plasma. *Lab Chip* 2015, 15, 113120, doi:10.1039/C4LC00809J.
- [10] Stefan Sinn, M. H.; Sinn, S.; Zeilinger, M.; Northoff, H.; Lieberzeit, P. A.; Gehring, F. K. Blood Coagulation Thromboplastine Time Measurements on a Nanoparticle Coated Quartz Crystal Microbalance Biosensor in Excellent Agreement with Standard Clinical Methods. *J. Biosens. Bioelectron.* 2013, 4, 16, doi:10.4172/2155-6210.1000139.
- [11] Huang, C.-C.; Lin, Y.-H.; Liu, T.-Y.; Lee, P.-Y.; Wang, S.-H. Review: Study of the Blood Coagulation by Ultrasound. *J. Med. Biol. Eng.* 31, 7986, doi:10.5405/jmbe.893.
- [12] Voleisis, A.; Kazys, R.; Mazeika, L.; Sliteris, R.; Voleisiene, B.; Grybauskas, P. Ultrasonic method for the whole blood coagulation analysis. *Ultrasonics* 2002, 40, 1017.
- [13] Libgot-Call, R.; Ossant, F.; Gruel, Y.; Lermusiaux, P.; Patat, F. High Frequency Ultrasound Device to Investigate the Acoustic Properties of Whole Blood During Coagulation. *Ultrasound Med. Biol.* 2008, 34, 252264, doi:10.1016/j.ultrasmedbio.2007.06.018.
- [14] Plag, C.; Libgot, R.; Gruel, Y.; Patat, F.; Ossant, F. 10C-2 High Frequency Ultrasound Characterization of Blood Clotting Process: Results Obtained With Plasma and Whole Blood. In *2007 IEEE Ultrasonics Symposium Proceedings; IEEE, 2007; pp. 884887.*
- [15] Huang, C.-C.; Wang, S.-H.; Tsui, P.-H. In Vitro Study on Assessment of Blood Coagulation and Clot Formation Using Doppler Ultrasound. *Jpn. J. Appl.*

Phys. 2005, 44, 87278732, doi:10.1143/JJAP.44.8727.

[16] KhuriYakub, B. T.; Smits, J. G.; Barbee, T. Reactive magnetron sputtering of ZnO. *J. Appl. Phys.* 1981, 52, 47724774, doi:10.1063/1.329315.

[17] Goksen G. Yaralioglu; Ira O. Wygant; Theodore C. Marentis; and Khuri-Yakub, B. T. Ultrasonic Mixing in Microfluidic Channels Using Integrated Transducers. 2004, doi:10.1021/AC035220K.

[18] Yaralioglu, G. Ultrasonic heating and temperature measurement in microfluidic channels. *Sensors Actuators A Phys.* 2011, 170, 17, doi:10.1016/J.SNA.2011.05.012.

[19] Hankel, W.G. Uber die aktinound piezoelektrischen eigenschaften des bergkrystalles und ihre beziehung zu den thermoelektrischen. *Abh. Schs.* 1881, 12: 457.

[20] Curie, P. & J. Dveloppement, par pression, de l'electricit polaire dans les cristaux hmides faces inclines. *Comptes Rendus.* 1880, 91: 294-295.

[21] JeanMistral C., Basrour S. and Chaillout J. Comparison of electroactive polymers for energy scavenging applications *Smart Mater. Struct.* 2010, 19 085012.

[22] White, R.M. Voltmer FW. *Appl Phys Lett.* 1965, 7:314316.

[23] Grate, J.W.; Frye G.C. Acoustic wave sensors. In: Baltes H, Gpel W, Hesse J (eds) *Sensors update*, 1996, vol 2. Wiley-VCH, Weinheim.

[24] Wohltjen, H.; Dessy R. *Anal Chem.* 1979, 51:14581464.

[25] Wohltjen, H.; Dessy R. *Anal Chem.* 1979, 51:14651470.

[26] Wohltjen, H.; Dessy R. *Anal Chem.* 1979, 51:14701475.

[27] Roederer, J.E., Bastiaans, G.J. *Anal Chem.* 1983, 55:23332336.

[28] Calabrese, G.S.; Wohltjen, H.; Roy, M.K. *Anal Chem.* 1987, 59:833837.

[29] Andle, J.C.; Vetelino, J.F. *Sens Actuators.* 1994, A 44:167176.

[30] Shons, A.; Dorman, F.; Najarian, J. *J Biomed Mater Res.* 1972, 6:565570.

[31] Thompson M.; Arthur C.L.; Dhaliwal G.K. *Anal Chem.* 1986, 58:12061209.

[32] Davis KA; Leary TR. *Anal Chem.* 1989, 61:12271230.

[33] Janshoff A; Steinem C. Quartz crystal microbalance for bioanalytical applications. In: Baltes H, Hesse J, Korvink JG (eds) *Sensors update*. 2001, vol 9. Wiley-VCH, Weinheim.

[34] Cooper MA; Singleton VT. *J Mol Recognit.* 2007, 20:154184.

[35] IEEE Standard on Piezoelectricity (1987), ANSI/IEEE Std 176

[36] A. Ballato (2001) Modeling piezoelectric and piezomagnetic devices and structures via equivalent networks, *IEEE Trans. Ultrason. Ferroelect, Freq. Contr.* 48(5):1189-1240

[37] G.S. Kino (1987) *Acoustic waves: devices, imaging, and analog signal processing* Prentice Hall, Englewood Cliffs, NJ

[38] V.M. Ristic (1983) *Principles of acoustic devices* John Wiley and Sons

[39] B.A. Auld (1990) *Acoustic fields and waves in solids*, Krieger Publishing Company

[40] W.P. Mason (1948) *Electromechanical transducers and wave filters* Van Nostrand, New York

[41] M. Redwood (1961) Transient performance of a piezoelectric transducer *Journal of the Acoustical Society of America* 33(4):327-336

[42] R. Krimholtz, D.A. Leedom, G.L. Mathaei (1970) New equivalent circuits for elementary piezoelectric transducers *Electronic Letters* 6(13):398-399

- [43] J. M. Thomson, blood coagulation and haemostasis, new york. Churchill livingstone, 1991.
- [44] R. Libgot-Calle, F. Ossant, Y. Gruel, P. Lemusiaux, F. Patat, High Frequency Ultrasound Device to Investigate the Acoustic Properties of Whole Blood During Coagulation, *Ultrasound Med.* 2008
- [45] R. Calle, G. Y. Rochefort, N. Desbuads, C. Plag, D. Antier, F. Ossant. Evaluation of the Sensitivity of a Murine Model. *Ultrasound Med.* 2010.
- [46] A. Voleisis, R. Kazys, B. Voleisiene, R. Sliteris, L. mazeika, Ultrasound Method for Monitoring the Clotting Process During Whole Blood Coagulation. *Ultrasounds.* 2017.
- [47] S.F. Nabavi, Portable Devices For In Vitro Characterization Based On Ultrasound. M.Sc. Thesis, 2015.
- [48] C. C. Huang, S. H. Wang, P. H. Tsui. Detection of Blood Coagulation and Clot Formation Using Quantitative Ultrasonic Parameters. *Ultrasound Med.* 2005.

VITA

Negar Majidi was born in Maragheh, Iran, in 1989. She received the B.Sc. in Electrical and Electronics Engineering - Biomedical Engineering (Bioelectric) from Sahand University of Technology, Tabriz, Iran, in 2013. Currently she is doing her M.Sc. in Electrical and Electronics Engineering at ÖZYEĞİN University, Istanbul, Turkey. Her current research interests include MEMS, Biosensors, ultrasound imaging, and signal processing.

During her education, she has contributed in authorship/co-authorship of 5 international conference and journal publications. Some portions of this dissertation have been submitted to IUS 2018 conference and an OA journal.